T-2530

THERMOELECTRIC PROPERTIES OF AMORPHOUS Sb AND Te

by

Douglas S. Peters

A thesis submitted to the Faculty and the Board of Trustees of the Colorado School of Mines in partial fulfillment of the requirements for the degree of Master of Science (Physics).

Golden, Colorado

Date: September 10, 1981

Signed: Doug Peters

Douglas S. Peters

Approved: J. U. Trefny

Dr. J. U. Trefny
Thesis Advisor

Golden, Colorado

Date: 9/10/81

F. D. Schowengerdt

Dr. F. D. Schowengerdt
Head, Department of Physics

ABSTRACT

An apparatus was designed and built for the in-situ measurements of the thermopower and resistance of amorphous thin films. These measurements have been made for amorphous Sb and Te over the temperature range 100 - 320 K. The temperature dependences of both quantities in amorphous Sb were consistent with the variable-range hopping model below 170 K. The density of states calculated from the resistance data of the Sb was in fairly good agreement with previously published results. The sign and temperature dependence of the thermopower of the Sb were found to vary strongly with preparation conditions. The Te results were considered more preliminary.

TABLE OF CONTENTS

LIST OF FIGURES

LIST OF TABLES

ACKNOWLEDGMENTS

I would like to sincerely thank my thesis advisor and teacher, Dr. John Trefny, whose patience and insight made this a very rewarding effort. Thanks also to Dr. Don Williamson and Dr. Art Sakakura for serving on my thesis committee.

I gratefully acknowledge the assistance of Dr. Jim Lockhart, who gave many valuable clues during the development of my apparatus, and Jack Kintner, whose expertise as a machinist helped make the design a reality.

I am also indebted to the National Science Foundation and the Colorado School of Mines for the financial aid I received during my studies.

I sincerely appreciate the moral and financial support of my parents. A special thanks to Lin Galasso who helped pull me through many difficult situations.

I. INTRODUCTION

A. Background

Amorphous Sb and Te, along with some other amorphous semiconductors, have come into the limelight recently because of their promise for various technological applications. This, coupled with the relative economy of fabricating amorphous materials as compared with crystalline materials, makes them very desirable objects of study.

Although the processes underlying thermoelectricity and conduction in crystalline solids are fairly well understood, no such single theory exists as yet for amorphous solids. Such a theory is sought after, not only by the physicist who wants to understand fundamental physical processes, but also by the practical mind, who sees in this understanding a possible means of improving the efficiency of thermoelectric and other devices.

Variable-range hopping has been suggested as the mechanism for conduction in amorphous Sb by Hauser (1) and in amorphous Te by Phahle (2). These conclusions were drawn from the temperature dependence of the resistivities of the two materials. However, no data were taken on the thermopowers. Further, the measurement of the resistances of these films took place in devices separate from the evaporation chambers, meaning a necessary exposure to handling and atmosphere.

B. Objectives

The purpose of this research effort was to provide simultaneous, in-situ measurements of the conductivity and the thermopower of evaporated, amorphous, Sb and Te films. A large part of the work went into the design and construction of the experimental apparatus, and the development of a method for obtaining both the films themselves, and the desired measurements. The results acquired thus far, although encouraging, should be considered as preliminary and are intended to be used as a guide for future work in this area.

C. Definition of Thermopower

A temperature gradient in a long, thin bar is accompanied by a gradient in the electric potential (Figure 1a). The constant of proportionality is the Seebeck coefficient, S (also called the thermopower), defined such that:

$$S = -\vec{\nabla} V / \vec{\nabla} T$$

Measurement of the Seebeck coefficient is performed as shown in Figure 1b, with no current flow. Note that because most materials exhibit a finite Seebeck coefficient, the measured E is not $V_1 - V_2$, but can include a contribution from the leads themselves.

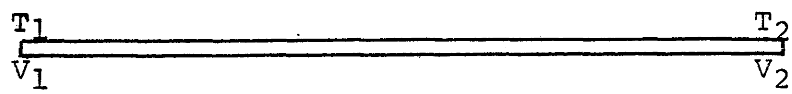

Figure 1a: The difference in potential generated between ends of a long, thin rod with the ends fixed at two temperatures.

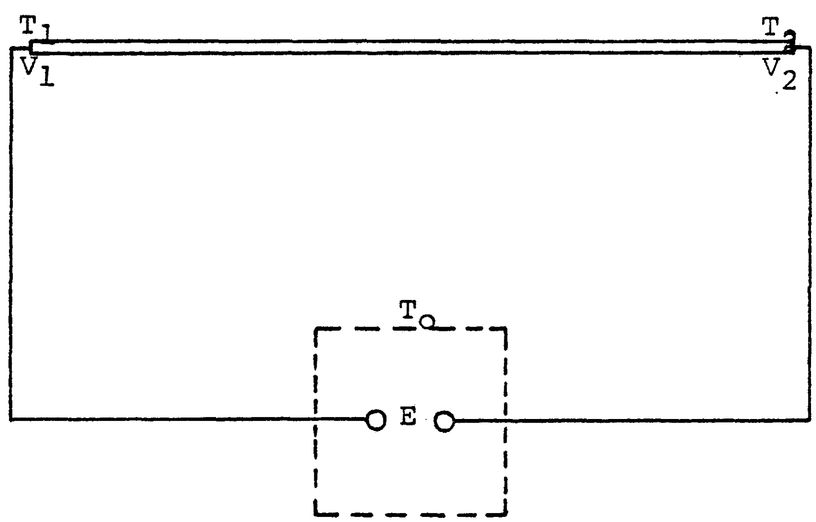

Figure 1b: Measurement of the thermoelectric voltage.

II. DESIGN AND DEVELOPMENT OF APPARATUS

A. Cold Traps

The original vacuum system consisted of a bell jar and a base plate with several feed-throughs: four to power evaporation boats, one for a thermocouple, one for a mechanical shutter and one for the LN_2 coolant. The substrate holder was mounted on a copper plate which was soldered in intimate thermal contact with the LN_2 feed-through tubes. A two inch inside diameter diffusion pump and a standard forepump were used to exhaust the system. This arrangement proved to be deficient in some respects, resulting in several modifications.

First, the lowest pressure attainable was 5×10^{-3} Pa (4×10^{-5} torr), two orders of magnitude higher than is common for systems involved in this type of work (1). Severe problems were encountered because of gettering onto the substrate when it was cooled to LN_2 temperatures in preparation for the evaporation. It was found that the evaporant would not adhere to the substrate because of the contamination. In addition, diffusion pump oil had been detected in the bell jar.

In an attempt to alleviate these problems, a cold trap was designed, built and installed between the bell jar and the diffusion pump (Figures 2, 3). The design of the cold trap centered around baskets containing zeolite which were cooled by steel LN_2 feed-through tubes. However, it proved impossible to make a leak-tight weld between the feed-throughs and the inner steel tube.

Because of this problem, the cold trap was re-designed and rebuilt (Figure 4). In this model, the zeolite was lacquered to the upper side of four copper semi-disks which were held firmly in contact with the inner tube of the LN_2 reservoir by turnbuckles. Indium wire and Wood's metal were used at the surface of contact for enhanced thermal conduction. This design exhibited insufficient cooling of the zeolite and hence not enough gettering to be of any use.

The final design of the cold trap, as suggested by Dr. J. M. Lockhart, is shown in Figure 5. The LN_2 reservoir is held by its exhaust and filling tubes directly in the pumping path. With this cold trap and a new four inch inside diameter diffusion pump, a pressure of 5×10^{-4} Pa(4×10^{-6} Torr), is attainable. The backflow of diffusion pump oil into the bell jar has also been stopped, or at least greatly reduced.

B. <u>Sample Holder and Thermocouples</u>

For the in-situ measurements of resistance and thermopower to be made, a substrate mount was designed and built (Figure 6). The Mylar substrate was suspended between clamps made of copper blocks. Chromel-Constantan thermocouples were soldered inside the copper blocks for measurement of temperature at either end. At each end, a copper plate, attached with copper wire to the block, was held down firmly against a copper pad previously evaporated onto each end of the substrate. After the sample had been evaporated onto the region between the two pads, this arrangement allowed for the measurement of the resistance across the sample and its thermoelectric power relative to Constantan and to Chromel. Two 100 ohm resistive heaters embedded in one of the copper blocks provided a temperature gradient across the sample. The entire mount was held firmly by brass screws against a copper plate which in turn was soldered to the LN_2 feed-through tubes. A thin coating of Corning vacuum grease was used at the holder-plate interface to enhance the thermal contact. Because of the poor thermal conductivity and small heat capacity of Mylar, the substrate tended to overheat in this configuration, producing a polycrystalline rather than an amorphous film.

The substrate mount was re-designed and built as shown in Figure 7. The substrate was held firmly against the aluminum mount by two copper plates which had been polished with 600 grit emery paper for good electrical and thermal contact. Thermocouples were soldered to each plate which were in turn varnished to bakolite blocks to prevent damage to the thermocouple junctions during handling. The entire assembly, including an Al mask to prevent stray electrical bridges, was then held firmly in place with nylon screws. The materials, thin copper plates, bakolite, nylon screws and aluminum mask were chosen to minimize the thermal mass of the thermocouple assemblies. One end of the mount was held firmly in contact with a copper base plate by brass screws. Vacuum grease was used at the surface of contact for better heat conduction. The other end of the mount was suspended in space and had a 100 ohm resistive heater embedded in it to provide the temperature gradient. The base plate was pressed against the LN_2-cooled holder by means of a supporting bracket during the cooling and evaporation phase (Figure 8). A layer of copper braid between them ensured good thermal contact. The bracket was then pivoted out from underneath the assembly to allow it to fall free for the measurement phase, which was done while the assembly slowly warmed to room temperature. Two supporting nylon screws provided good thermal insulation during the warm-up to assure that it was slow.

C. Miscellaneous

The original two-lead thermocouple feed-through was replaced by one with four leads. This provided Chromel and Constantan leads which were continuous from the thermocouple junctions to a constant temperature oil bath where the switching between various leads took place (Figure 9 and below).

The seal on the LN_2 feed-throughs leaked at low temperatures; it was re-designed, built and installed. Finally, because of instabilities in the original, a new ion gauge and gauge control was installed.

The substrate mount in position for evaporation (shown without the supporting bracket) is shown in Figure 10.

Al_2O_3 boats powered by an AC supply were used for the evaporation. (See Appendix D for power settings).

Electrical measurements were made with a Keithly 191 Digital Multimeter.

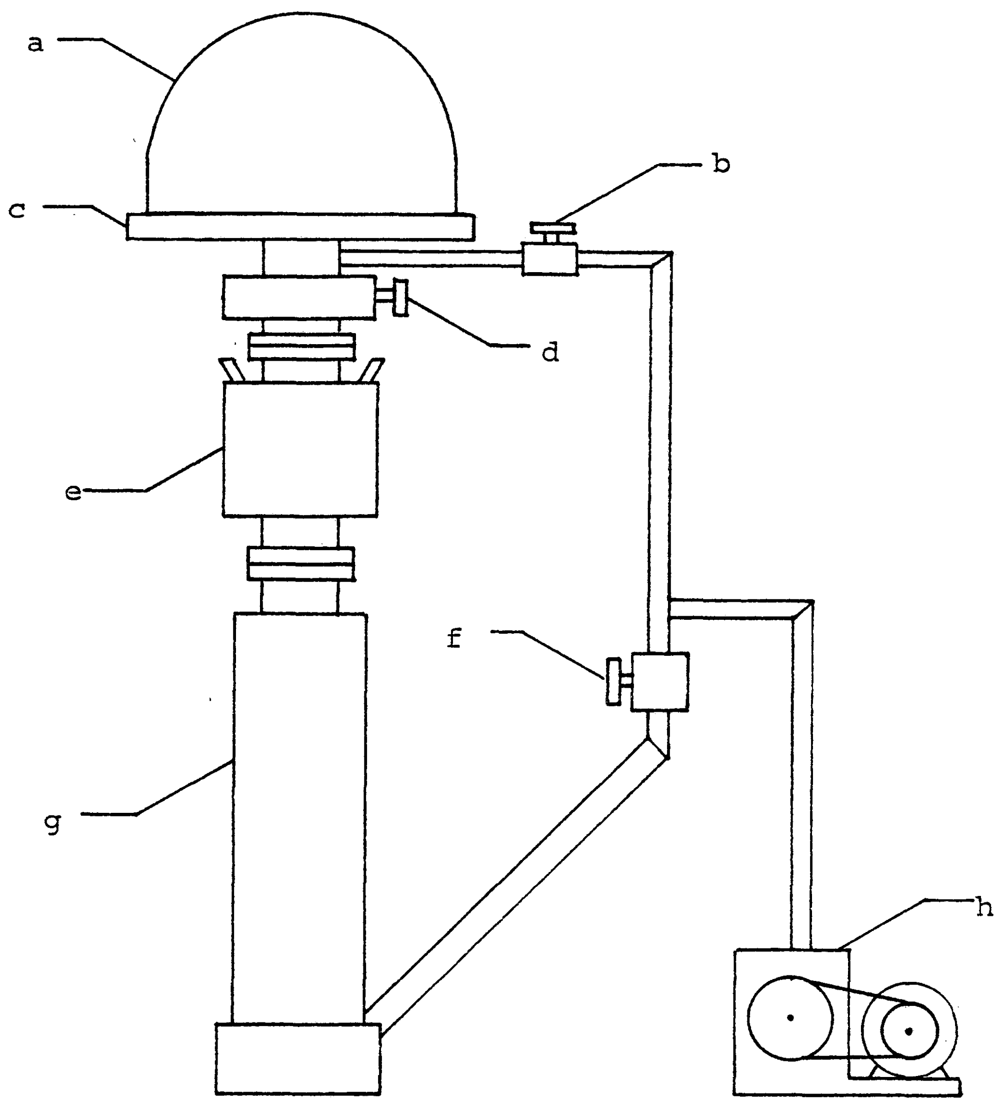

Figure 2: Vacuum System. (a-bell jar, b-bell jar rough-out valve, c-base plate, d-gate valve, e-cold trap, f-diffusion pump valve, g-diffusion pump, h-mechanical pump).

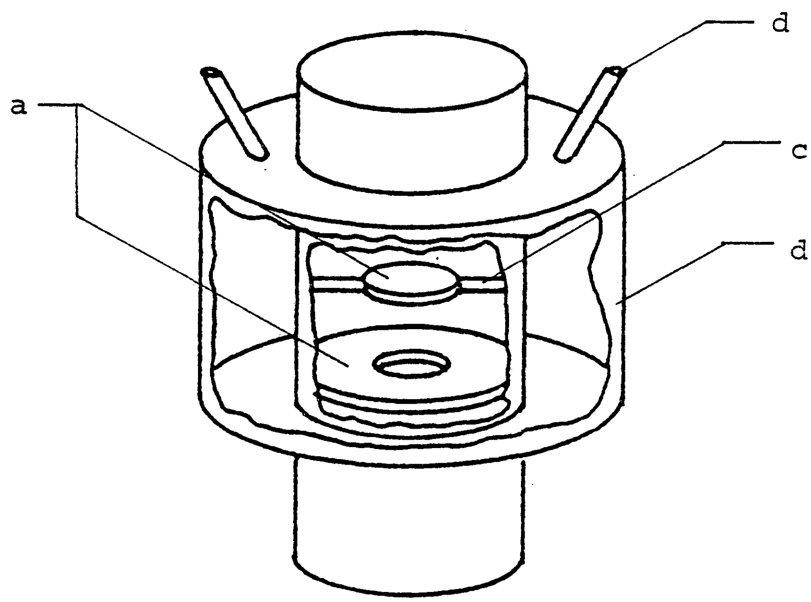

Figure 3: Cold Trap I. (a-baskets containing zeolite, b-LN_2 reservoir, c-steel feed throughs, d-reservoir fill and exhaust tubes).

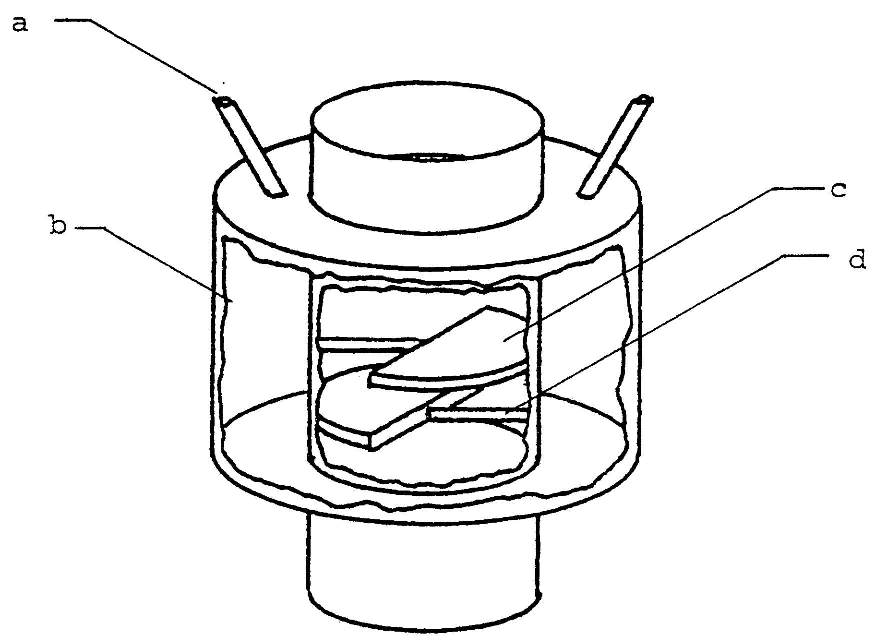

Figure 4: Cold Trap II. (a-reservoir fill and exhaust tubes, b-LN_2 reservoir, c-copper semi-disks with zeolite lacquered to top, d-turnbuckles).

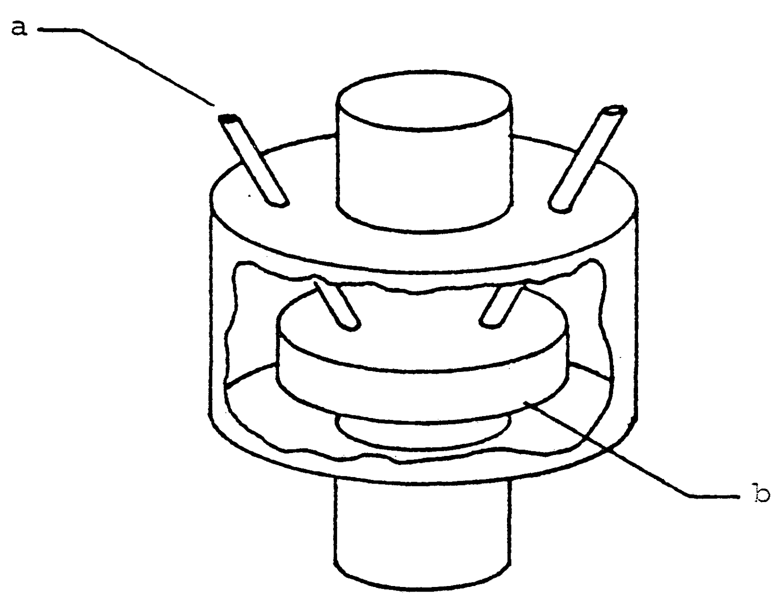

Figure 5: Cold Trap III(Final). (a-reservoir fill tubes and supports, b-LN_2 reservoir).

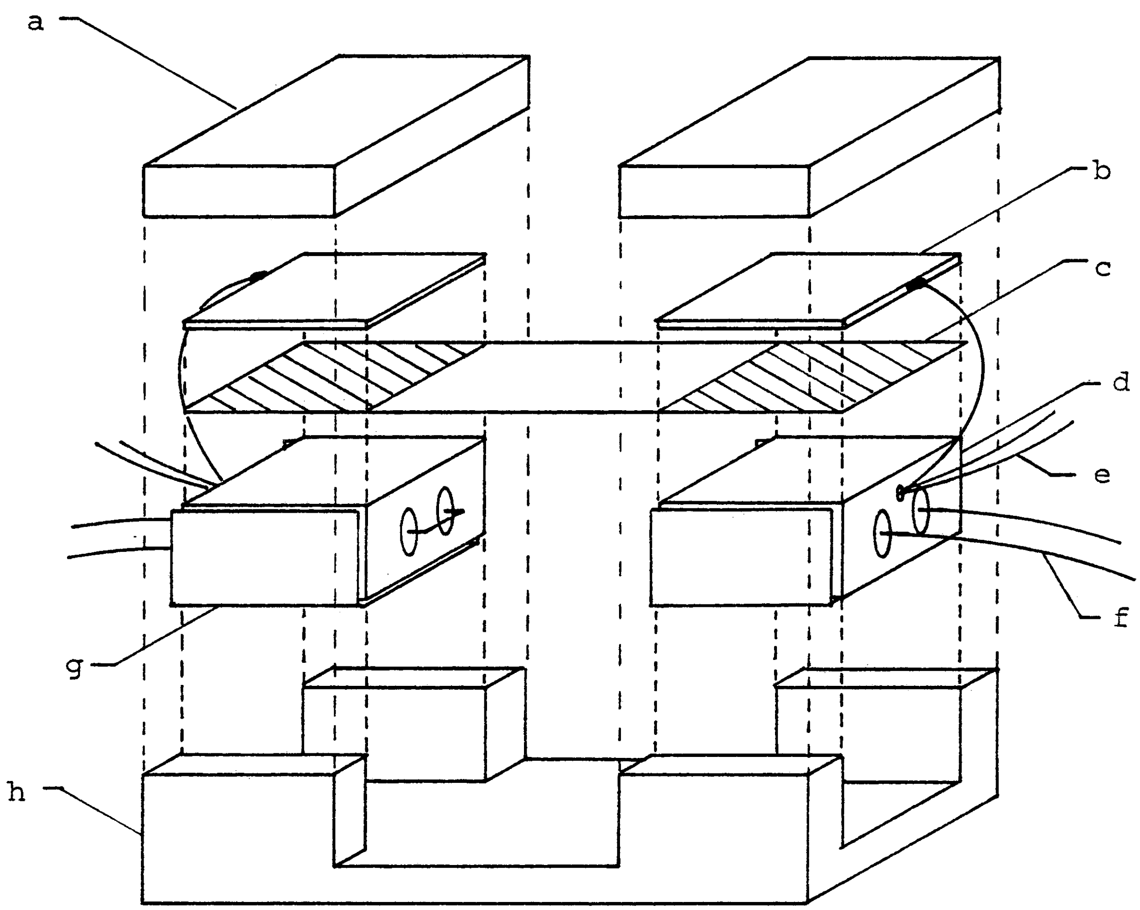

Figure 6: Holder I. (a-bakolite, b-copper plate, c-substrate w/copper end pads, d-copper block, e-thermocouple leads, f-resistive heater leads, g-Mylar insulator, h-aluminum base.)

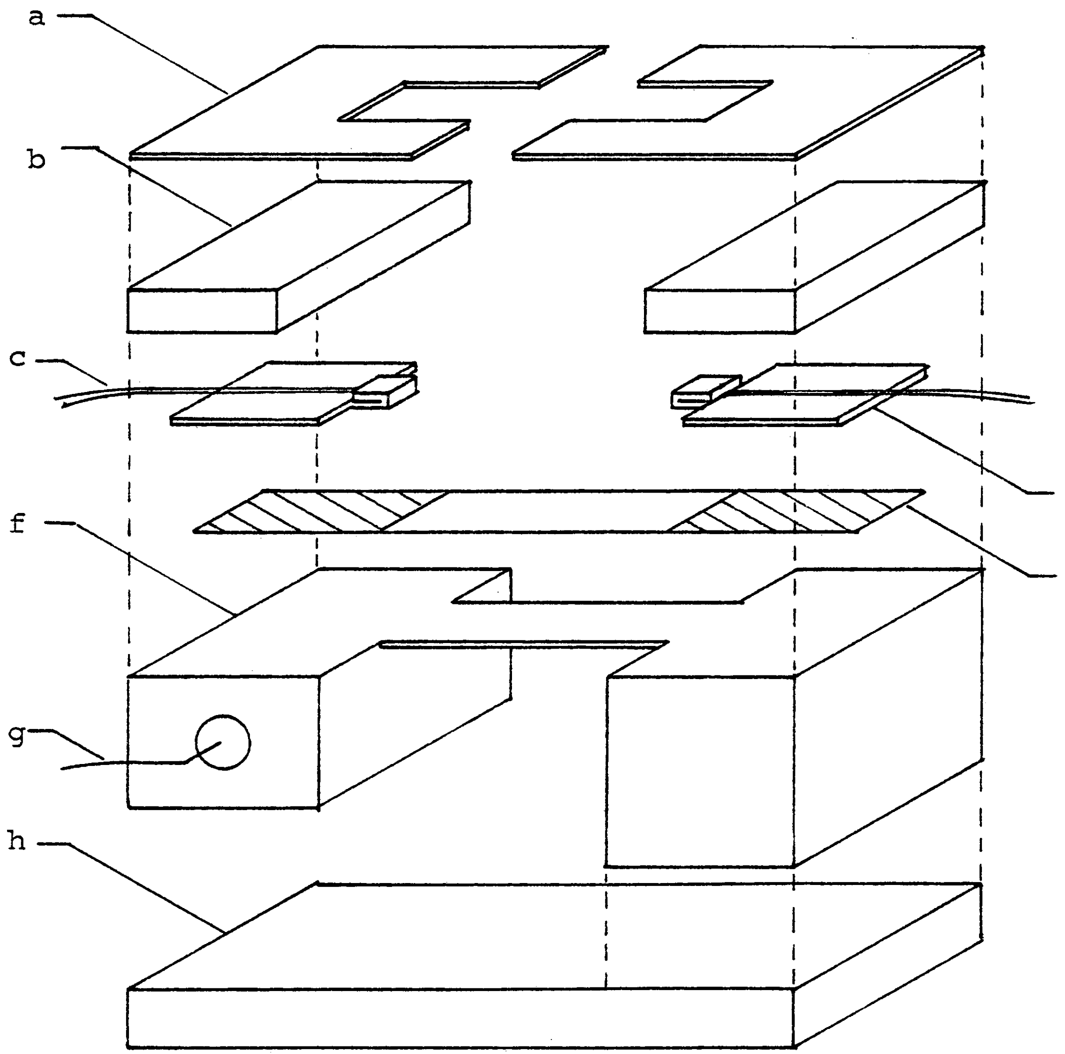

Figure 7: Holder II. (a-aluminum mask, b-bakolite, c-thermocouple leads, d-copper plate, e-substrate w/copper end pads, f-aluminum mount, g-resistive heater leads, h-copper base plate).

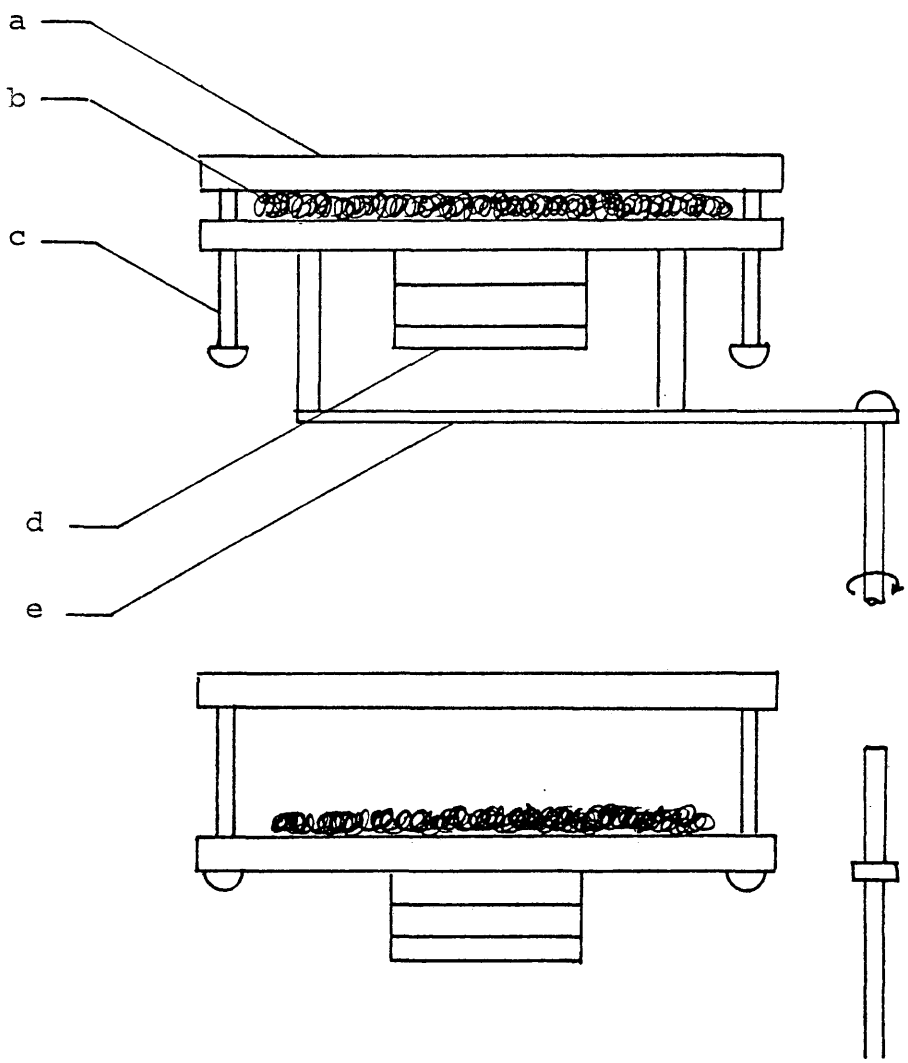

Figure 8: Support Bracket. Top: Assembly in position for cooling. Bottom: Assembly dropped for warming. (a-LN_2 cooled holder, b-copper braid, c-nylon screws, d-substrate mount, e-support bracket.)

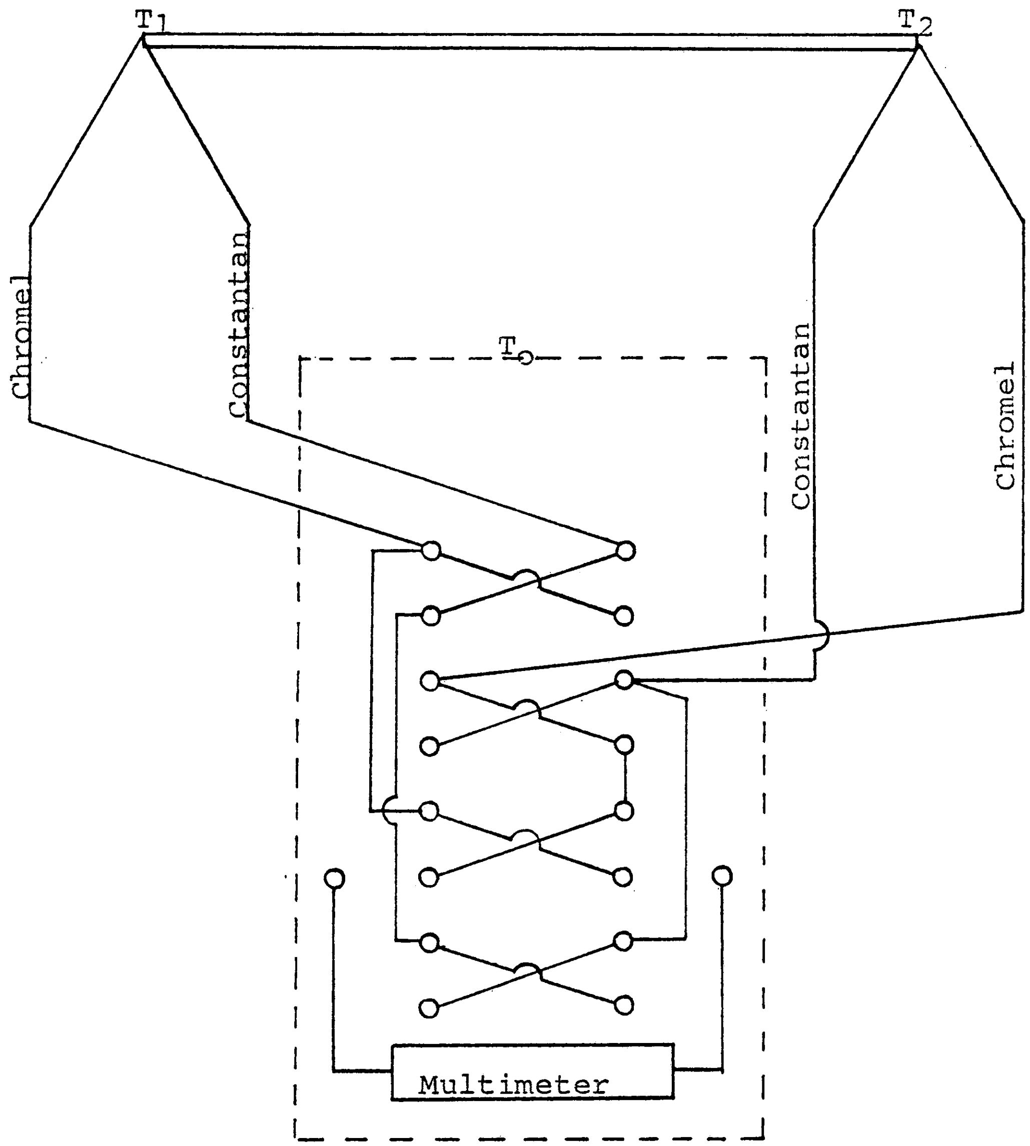

Figure 9: Circuit Diagram. Switching done by a mechanical multi-position switch immersed in a constant temperature oil bath.

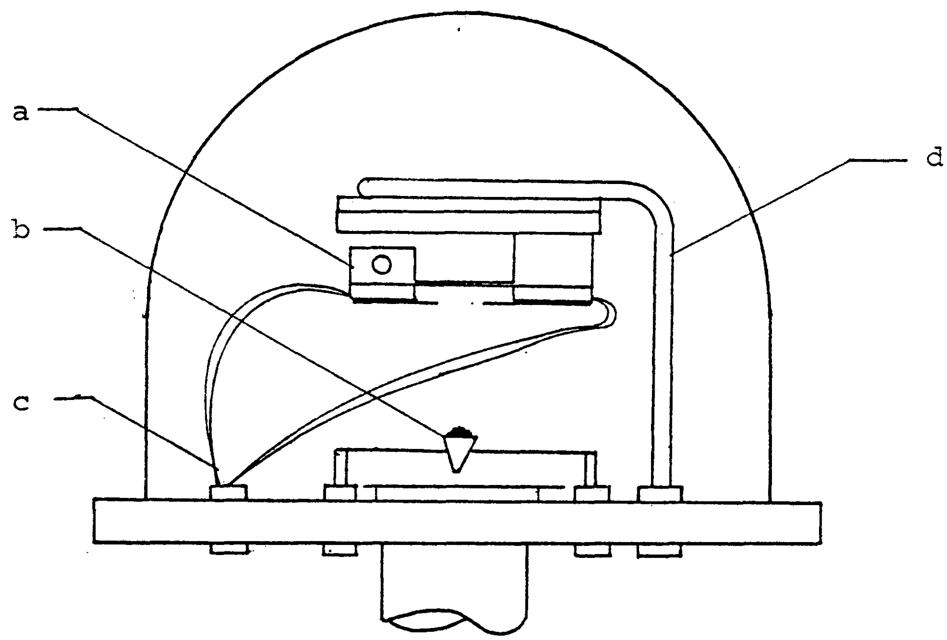

Figure 10: Bell-Jar Assembly. (a-substrate mount, b-boat, c-thermocouple leads, d-LN_2 feed-throughs.)

III. EXPERIMENTAL PROCEDURE

The experimental procedure can be divided into four parts: preparation and mounting of the substrate, pumping down of the system, evaporation of the sample, and measurement of the thermoelectric power and resistance of the sample.

A. Mounting and Preparation of Substrate

The substrate used was 2.5 micron thick Mylar. 200 micron thick glass slides were also tried by did not prove suitable, as the evaporated films did not adhere well at low substrate temperatures.

Copper pads were evaporated onto the two ends of the substrate to allow good electrical contact between the thermocouple plates and the sample. Acetone originally was used to clean the surface in preparation for evaporation of the film, but this seemed to leave a residue which inhibited its adhesion to the substrate. Because of this, the method chosen for cleaning the substrate was simply to run a stream of presurized nitrogen gas across the surface to remove large particles of dust.

The substrate was mounted flush against the metal substrate holder for good thermal contact. This allowed for proper cooling of the substrate during the evaporation. A thin coating of Corning vacuum grease between the substrate and substrate holder was used on several occasions to enhance the thermal contact, but the films produced in this manner showed severe cracking and peeling, perhaps due to stress caused by contraction and freezing of the grease upon cooling.

B. Pumpdown

During the pumpdown, care was taken to keep organics from the diffusion pump from reaching the bell jar. With the gate valve and the bell jar rough-out value (Figure 2) closed, the diffusion pump was evacuated via the diffusion pump valve to below 2.7 Pa (20mT). Then the diffusion pump valve was closed and the bell jar rough-out valve was opened to evacuate the bell jar. Once the pressure was below 2.7 Pa (20mT), welding grade Argon was introduced to increase it again to 100 Pa (750mT). This was followed again by an evacuation to 2.7 Pa (20mT). This purging cycle was repeated three times. On some samples (see Table 1) the boat was gently heated (variac setting 30) for three minutes before the final purging to remove oxides from the un-evaporated charge.

When the pressure in the bell jar was below 2.7 Pa after the final purging, the bell jar rough-out valve was closed and the diffusion pump valve opened. The cold trap was then filled with LN_2 and power was supplied to the diffusion pump. After the diffusion pump reached operating temperature, typically about 30 minutes, the cold trap was topped off and the gate valve opened. The system then required 2 to 4 hours to reach the base pressure of 5×10^{-4} Pa (4×10^{-6} Torr).

C. Evaporation

At this point LN_2 was pumped through the holder until the desired substrate temperature for evaporation was reached (see Table 1). On all samples made before 7/26/81, the boat was heated (variac 30) for 3 minutes before the shutter was opened. On samples made on and after 7/26/81, there was no shutter. The power to the boat was slowly increased as the evaporation progressed. The average boat power and evaporation time for the various samples are given in Table 1. After completion of the evaporation, LN_2 was again fed to the substrate holder to cool the sample as far as possible.

D. Measurements

On all samples except Sb No. 6, the measurement procedure was as follows. The power supply to the resistive heater was set at .5W (5 volts). The LN_2 was shut off to allow the sample to warm slightly, then turned on momentarily to halt the warming. The measurements had to be taken quickly and timed so that the holder was roughly at equilibrium. This method of taking measurements was extremely difficult and time consuming, resulting in the design of the bracket shown in Figure 8. This design allowed the entire holder and substrate to warm slowly, less than 0.5 K/min. On Sb No. 6, the substrate and holder were allowed to warm slowly and continuously to room temperature with the newly designed holder.

The specific meter readings and their relationships to the reported sample properties are discussed in detail in Appendix A.

Table 1: Evaporation Conditions

Sample	Date (1981)	Substrate Evaporation Temp. (K)	Base Pressure	Evaporation Pressure	Average Variac Setting	Evaporation Time (min)
Sb No.1	5/27	208	7.0×10^{-6}	8.2×10^{-6}	30.5*	5 (3)
Sb No.2	6/2	215	2.2×10^{-6}	3.6×10^{-6}	33.5*	11 (8)
Sb No.3	6/9	219	4.2×10^{-6}	1.2×10^{-5}	35.3	21 (19)
Sb No.4	6/16	208	1.6×10^{-6}	4.1×10^{-6}	33.5*	9 (3)
Sb No.5	6/17	207	3.2×10^{-6}	5.0×10^{-6}	32.8*	10 (17)
Sb No.6	7/26	110	2.3×10^{-6}	5.0×10^{-6}	31	27 (2)
Sb No.7	8/5	190	1.3×10^{-6}	9.2×10^{-6}	50	18 ?
Te No.1	6/19	206	2.8×10^{-6}	5.0×10^{-6}	31	7 ?

Under evaporation time, the first number represents the number of minutes that the shutter was open. The number in parenthesis is the length of time after the first finite resistance was recorded that the evaporation continued.

*Boat heated in Argon at 20 mT for 3 minutes.

IV. EXPERIMENTAL RESULTS

A. Amorphous Sb

The raw data was converted as shown in Appendix A, and the results are tabulated in Appendix B.

The behavior of the resistance vs. temperature for Sb is shown in Fig. 11. Only samples 1, 5, and 7 are plotted for clarity, but this behavior was consistent for all of the amorphous Sb samples up to their crystallization temperatures, about 220-270 K. At that temperature, the resistance abruptly dropped from the order of kilohms to the order of ohms.

The behavior of the thermopower vs. temperature for a typical sample is shown in Fig. 12. Although the exact shape and value varied at low temperatures (see Discussion), the trend was always the same: from a positive Seebeck at low T to a small negative peak near the crystallization temperature. After crystallization, the Sb showed a small positive Seebeck Coefficient which was reproducible (see Appendix C).

B. Amorphous Te

The resistance vs. temperature and Seebeck Coefficient vs. temperrature for the lone Te sample are shown in Fig. 13 and Fig. 14, respectively. The data are also tabulated in Appendix B.

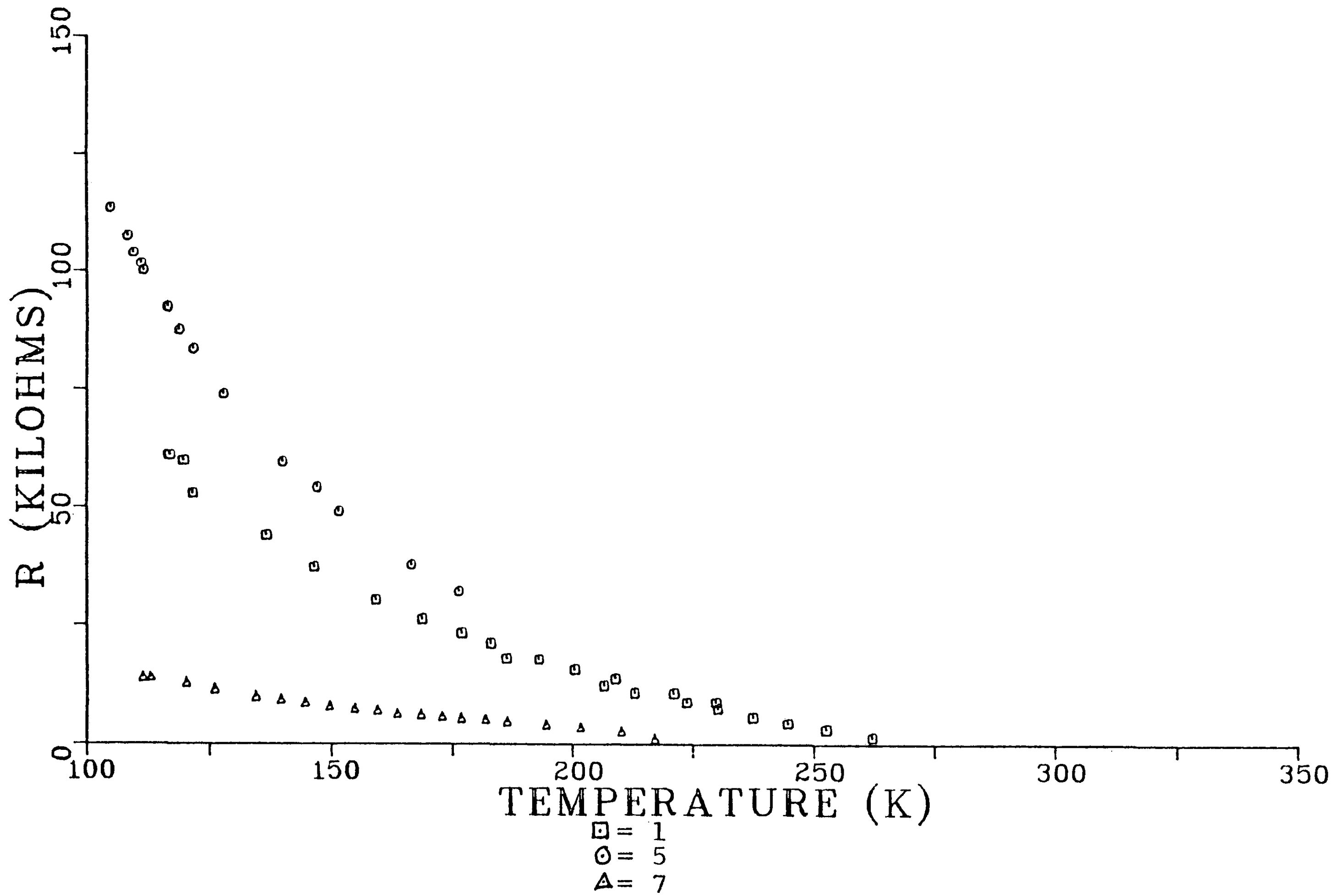

Figure 11: R vs. T for Sb No. 1, 5 and 7.

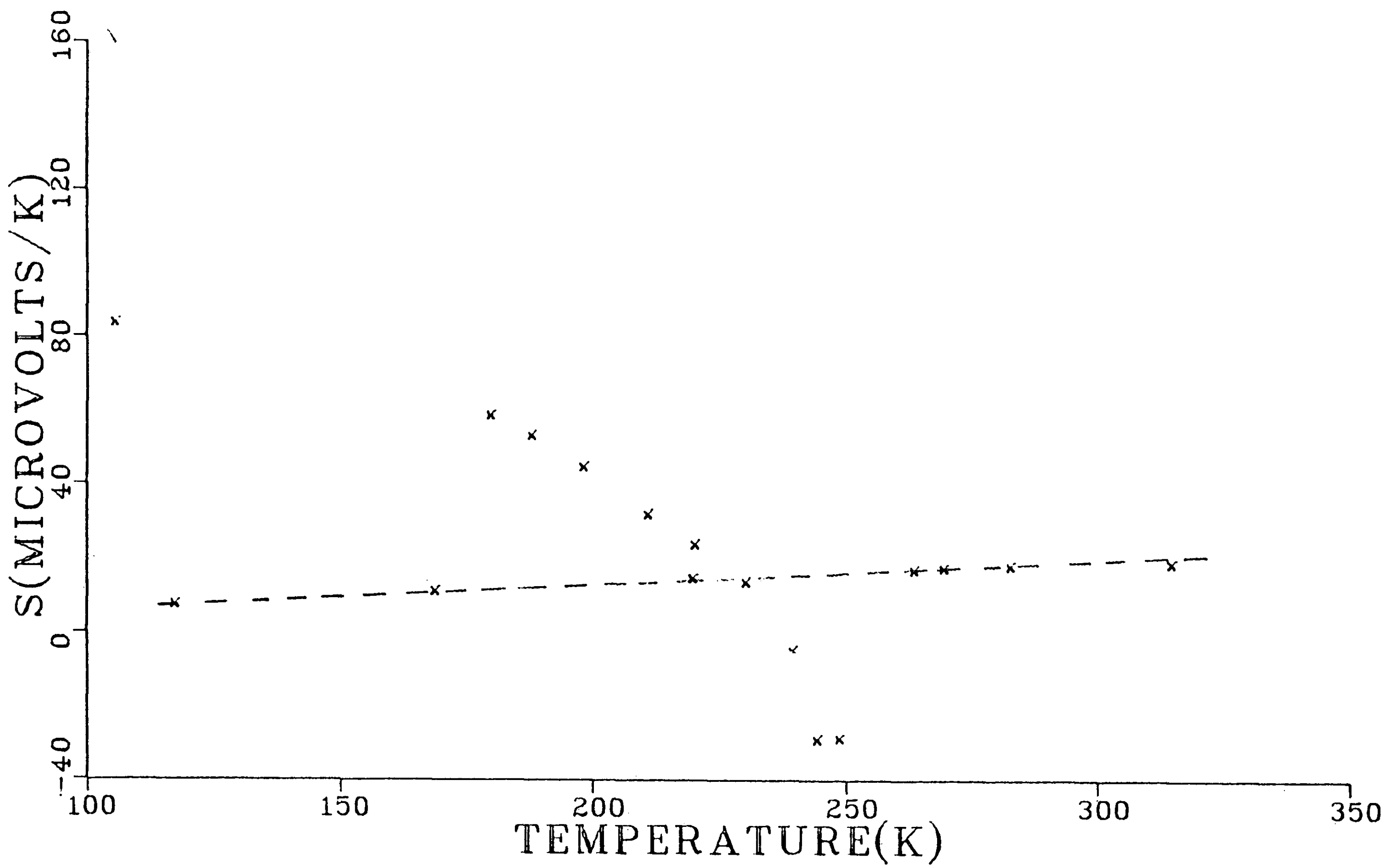

Figure 12: Seebeck Coefficient vs. Temperature for Sb No. 2. (Dashed line goes through points obtained after crystallization.)

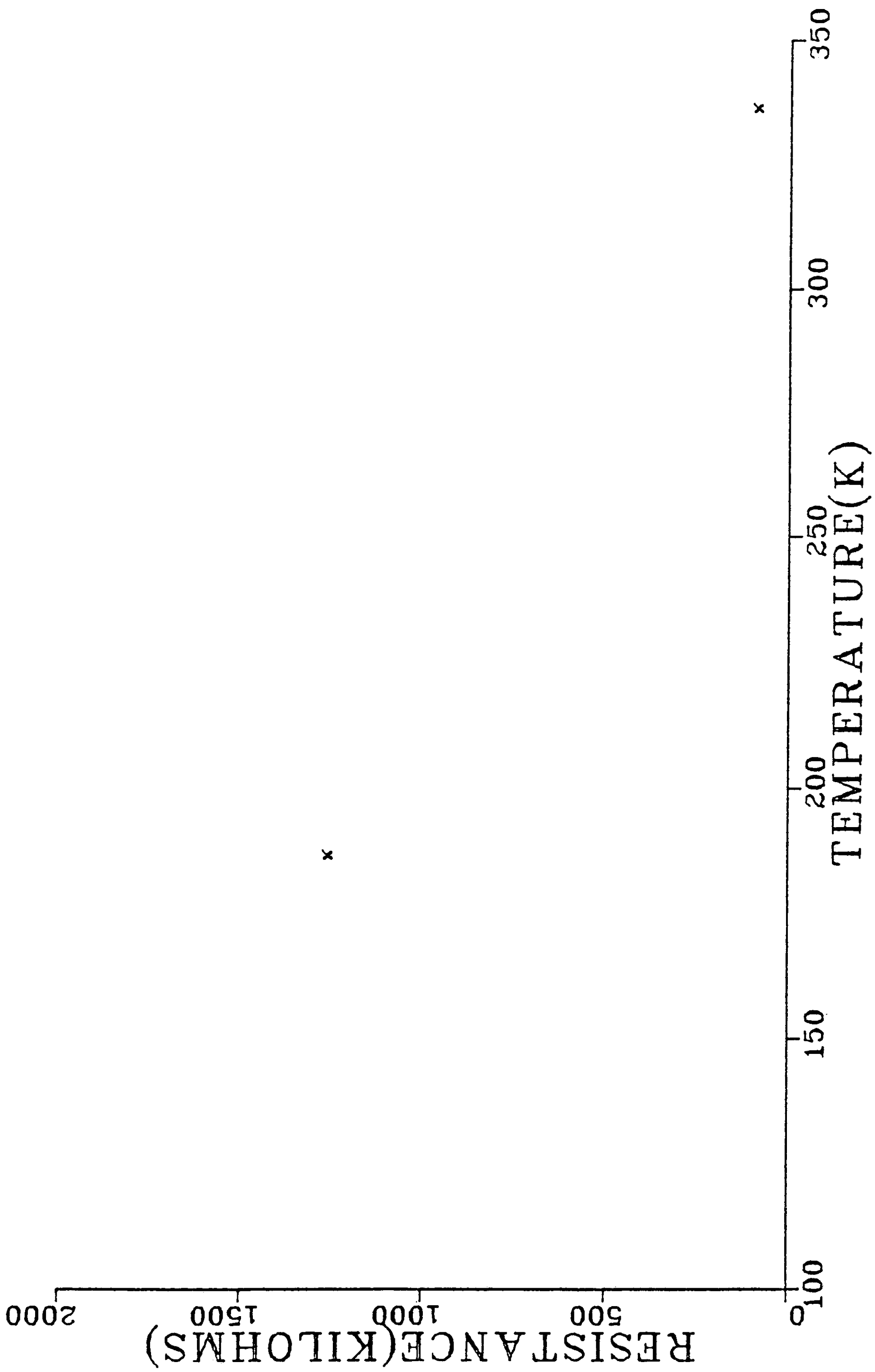

Figure 13: Resistance vs. Temperature for Te No. 1.

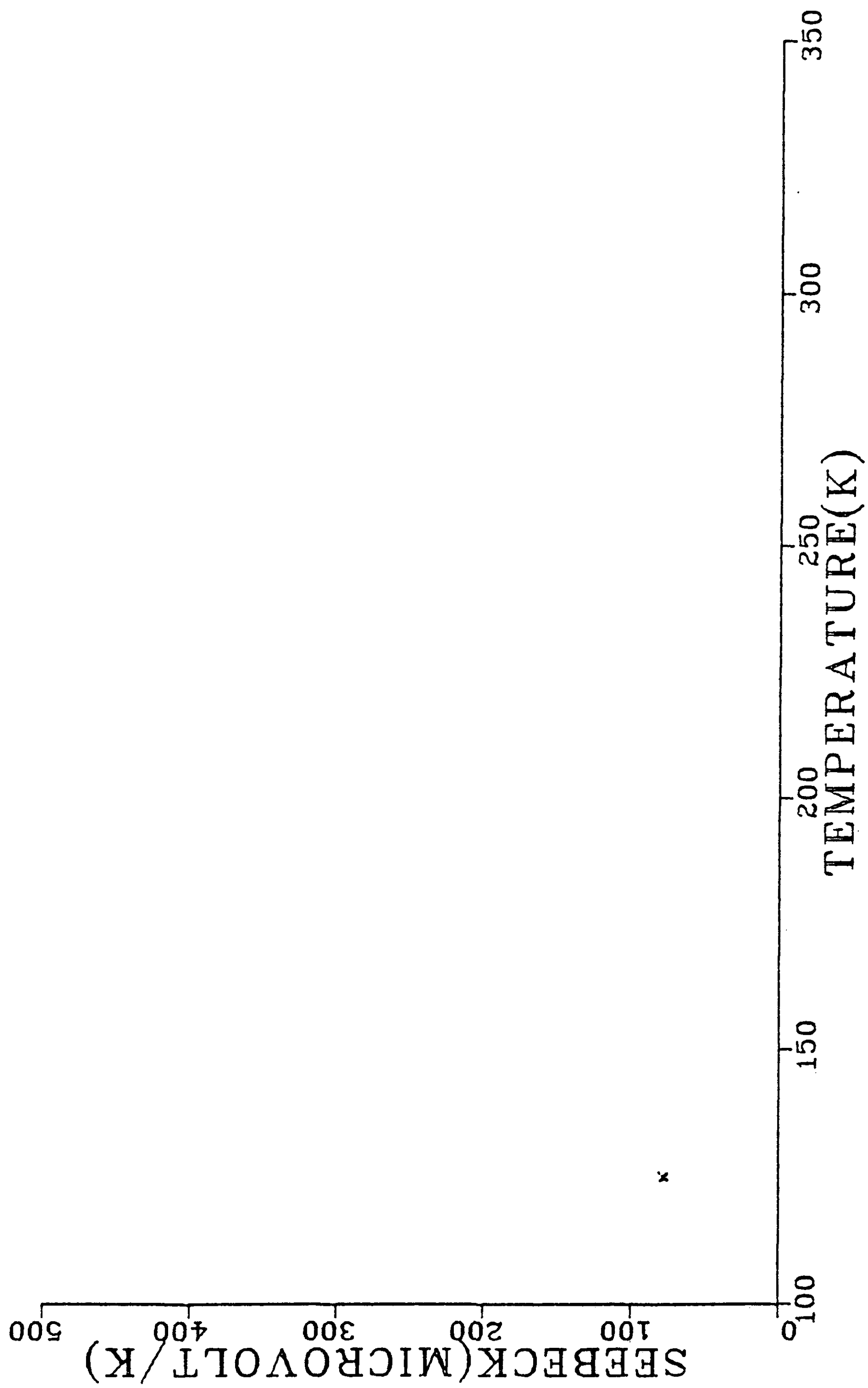

Figure 14: Seebeck Coefficient vs. Temperature for Te No. 1.

V. THEORY

A. Drude Theory of Metals (1900)

Before Thomson's discovery of the electron in 1897, the flow of electricity through a solid was considered as that of a fluid. But the new knowledge of the particulate nature of the charge carriers led Drude in 1900 to apply the kinetic theory of gases to electrons moving through a fixed ionic lattice.

In his simple model, Drude treated the electrons and ions as hard spheres subject to instantaneous collisions. Electron-ion scattering was considered predominant while electron-electron scattering was ignored. Except for collisions, all other interactions were ignored.

Thus, the electrons achieved thermal equilibrium only through collisions with the ions in the lattice. The velocity of the electron after the collision was considered independent of its velocity before and was governed by the local temperature through the Maxwell-Boltzmann distribution.

The probability of a collision per unit time for an electron was assumed to be $1/\tau$, a quantity independent of velocity and position within the crystal. This became known as the relaxation time approximation.

From Drude's model the following expressions for the conductivity (σ) and the thermoelectric power (S) were derived:

$$\sigma = \frac{ne^2\tau}{m}$$

$$S = \frac{-k}{2e}b = -43\,\mu V/K$$

Note that in the expression for σ, τ is treated as a parameter deduced from the experimentally measured conductivity of each metal. There is thus no formal understanding of τ. For a true test of Drude's theory, therefore, one must examine quantities independent of τ. The thermoelectric power is one such quantity. The theoretically predicted value for S is unfortunately several orders of magnitude too large for most metals. Further, in some metals the sign of S is actually positive.

B. Sommerfeld Theory of Metals (1925)

With the discovery of the principles of quantum mechanics in the early 1900's, it became clear that Maxwell-Boltzmann statistics was not appropriate for describing the high-density, low temperature "gas" of conduction electrons found in the typical metal at room temperature.

Sommerfeld reworked the Drude theory of metals with the single modification of replacing Maxwell-Boltzmann "classical" statistics with Fermi-Dirac "quantum" statistics. Otherwise, the electrons were still being described classically. A simple argument relating to the uncertainty principle provides the justification for using such a quantum-classical theory.

A typical conduction electron momentum is about equal to $\hbar k_F$. For a classical description, the uncertainty in the momentum, Δp, should be small compared to $\hbar k_F$. Thus,

$$\Delta x \sim \frac{\hbar}{\Delta p} >> \frac{1}{k_F} \sim r_s$$

where r_s is the mean interatomic spacing, on the order of angstroms. Therefore, the uncertainty in the electrons position must be large compared to the mean interatomic spacing. Valence electrons have as their domain the entire crystal volume. Further, at room temperature the typical mean free path is on the order of 100A, increasing with lower temperature. (Also note that a slowly varying external field is implied, which is true for most cases.) It is thus possible to use this hybrid quantum-classical model.

Sommerfeld derived the same expression for σ as Drude, but his result for S:

$$S = \frac{-\pi^2}{6} \frac{k_B}{e} \frac{k_B T}{E_F} \times 10^{-4} \text{ volt/K}$$

$$= -1.5 \mu V/K \quad \text{(at room T for a typical } E_F\text{)}$$

was in good agreement with the value for most normal metals. However, Sommerfeld still could not predict the temperature dependence of and the existence of a positive S for some materials remained inexplicable.

C. Theory of Amorphous Semiconductors

1. Anderson Localization

In the Bloch theory, the electronic wavefunctions span the entire volume of a perfectly periodic lattice. As disorder in the lattice increases, however, solutions of the Schrodinger equation become localized in space. This phenomenon was first proved theoretically by Anderson in 1958 (3). In his simple model, variations in the depths of the ionic potential wells were the source of the disorder, but the same result is obtained if the positions of the lattice sites are shifted randomly from perfect periodicity. The resulting electronic wavefunctions in this model decrease exponentially as $\exp(-\alpha r)$ with distance r from each site. The parameter α determines the strength of the localization. It should be noted that the electron therefore still has a finite probability of being found at nearby sites. Electronic motion in this situation takes place by discontinuous jumps from one localized state to another, hence the term "hopping".

2. Hopping Conductivity

When the electronic wave functions are strongly localized, hopping is to nearest-neighbor sites only. This gives rise to a conductivity

$$\sigma \propto e^{-c/T}$$

When the localization is weaker, variable-range hopping results, which gives

$$\sigma \propto e^{-c/T^{1/4}}$$

This is the case for amorphous Sb and Te. The following treatment is after Mott and Davis (3).

Assume that an electron will normally hop a distance less than some R, which is a function of temperature. This means the available volume is:

$$V = \frac{4}{3}\pi R^3$$

Now, from the definition of the density of states, N(E)dE is the number of states per unit volume with energy between E and E + dE. So the total number of states within the prescribed volume and between energies E and E + dE is:

$$\frac{4}{3}\pi R^3 N(E)dE$$

Hence, the average spacing between states is

$$\frac{3}{4\pi R^3 N(E)}$$

Now assume that the electron will normally jump to a site for which the activation energy, W, is lowest. Remembering that the hopping occurs for electrons within kT of the Fermi energy, $N(E) \simeq N(E_F)$, and

$$W = \frac{3}{4\pi R^3 N(E_F)}$$

The average hopping distance is

$$\bar{R} = \frac{\int^R r^3 dr}{\int^R r^2 dr} = \frac{3}{4}R.$$

The probability of a hop per unit time is thus

$$\nu_{ph} \exp(-2\alpha\bar{R})\exp(-W/KT),$$

the product of three factors: 1) the phonon frequency which is the number of "tries" per second that the electron has, 2) a factor accounting for the overlap of the wave functions, and 3) the "Boltzmann" factor accounting for the difference in energies of the two states. Maximizing the probability with respect to $\bar{R}$ and solving for $\bar{R}$ gives the most probable hopping distance.

The result is:

$$R = \left[\frac{3}{2\pi\alpha N(E_F)kT}\right]^{1/4}$$

The hopping rate is therefore

$$\nu_{ph}\exp(-B/T^{1/4}),$$

where $B = B_o\left[\frac{\alpha^3}{kN(E_F)}\right]^{1/4}$ and $B_o = 2(3/2\pi)^{1/4}$

Now consider the case with an applied electric field, F. The hopping rate against the field is

$$\nu_{ph}\exp\left[-2\alpha\bar{R} - \frac{W + e\bar{R}F}{kT}\right]$$

and the hopping rate with the field is

$$\nu_{ph}\exp\left[-2\alpha\bar{R} - \frac{W - e\bar{R}F}{kT}\right]$$

Thus the net hopping rate in the direction of the field is

$$\nu_{ph}\exp\left[-2\alpha\bar{R} - \frac{W - eRF}{kT}\right] - \nu_{ph}\exp\left[-2\alpha\bar{R} - \frac{W + eRF}{kT}\right]$$

$$= \nu_{ph}\exp\left[-2\alpha\bar{R} - \frac{W}{kT}\right]2\sinh\left(\frac{eRF}{kT}\right)$$

The number of electrons per unit volume within a range kT of the Fermi energy is on the order of $N(E_F)kT$. To get the current flow, multiply the net hopping rate in the direction of the field by the average hopping distance $\bar{R}$, the electronic charge e, and the number of hopping electrons, $N(E_F)kT$. Thus,

$$J = 2N(E_F)kT\bar{R}e\,\nu_{ph}\exp[-2\alpha\bar{R} - \frac{W}{kT}]\sinh\left(\frac{e\bar{R}F}{kT}\right)$$

For small fields $e\bar{R}F \ll kT$, so to first order

$$J \approx 2N(E_F)\bar{R}^2e^2\,\nu_{ph}F\exp[-2\alpha\bar{R} - \frac{W}{kT}]$$

$$= 2N(E_F)\bar{R}^2e^2\,\nu_{ph}F\exp(-B/T^{1/4}),$$

and since $\sigma = J/F$,

$$\sigma = 2N(E_F)R^2e^2\,\nu_{ph}\exp(-B/T^{1/4}).$$

different treatments give different values of B_0 (3), ranging from 2.5 to 1.7.

For his work with amorphous Sb, Hauser chose

$$B = \left(\frac{16\alpha^3}{N(E_F)k}\right)^{1/4}$$

3. Thermopower

In an applied electric field, F, the current in an amorphous solid is given by:

$$\bar{J}_Q = \sigma\bar{F}$$
$$= e\int n(\bar{k})\bar{v}d^3k.$$

The Boltzmann equation in the relaxation-time approximation is:

$$(\partial n/\partial t) + \bar{V}\cdot\bar{\nabla}_{\bar{R}}n + (\bar{F}/m)\cdot\bar{\nabla}_{\bar{V}}n = -(n-n_0)/\tau.$$

In equilibrium and steady state, the first two terms on the left drop out, giving for n:

$$n = n_o - (\bar{F}\tau/m)\cdot\bar{\nabla}_{\bar{v}}n$$
$$\simeq n_o - (\bar{F}\tau/m)\cdot\bar{\nabla}_{\bar{v}}n_o$$

to first order. This form of n, when substituted into the current integral gives, after application of the chain rule to the gradient operator and a change of variable in the integration

$$\sigma = -\int\sigma_E(\partial f_o/\partial E)\ dE,$$

where σ_E contains all 'leftover' terms. Hence, in an applied field the element of current by carriers with energies between E and E + dE is

$$-dJ = \sigma_E(\partial f/\partial E)FdE,$$

which carries free energy

$$-[(E-E_F)/e]dJ = (1/e)(\partial f/\partial E)\,\sigma_E(E-E_F)FdE.$$

Integrating over the range of energies of the carriers gives the total heat transport

$$(F/e)\int\sigma_E(\partial f/\partial E)(E-E_F)dE = J\Pi$$

where Π is the Peltier coefficient. Now, because $S = \Pi/T$ and $J = \sigma F$,

$$S\sigma = (k/e)\int\sigma_E\ [(E-E_F)/kT](\partial f/\partial E)dE.$$

A standard form for σ_E is

$$\sigma_E = e^2DN(E),$$

where D is the diffusion coefficient. The conductivity may then be written as

$$\sigma = -\int e^2DN(E)(\partial f/\partial E)dE$$

and

$$S\sigma = (k/e)\int e^2 DN(E)\ [(E-E_F)/kT](\partial f/\partial E)dE$$

so

$$S\ = -(k/e)\ \frac{\int N(E)[(E-E_F/kT)](\partial f/\partial E)dE}{\int N(E)(\partial f/\partial E)dE}.$$

Making the change of variable

$$x = (E-E_F)/kT,$$

the limits of integration are -W/kT to W/kT. The integrands in the numerator and denominator are then Taylor expanded about x = 0. This gives, to first order,

$$S = -(k/e)kT(\partial\ln N/\partial E)_{E_F}\ \frac{\int x^2(\partial f/\partial x)dx}{\int(\partial f/\partial x)dx}$$

But

$$\int(\partial f/\partial x)dx \simeq -1, \text{ for large } W/kT.$$

And

$$\int x^2(\partial f/\partial x)dx = 2(W/kT)^2 + \mathcal{O}(1)$$

after an integration by parts. This gives for the thermopower:

$$S \simeq 2(k/e)(W^2/kT)(\partial\ln N/\partial E)_{E_F}$$

This result is different from that given by Mott (3):

$$S = 1/2(k/e)(W^2/kT)(\partial\ln N/\partial E)_{E_F} + (k/e)\ln 2.$$

For variable-range hopping,

$$W^2/(kT) = K(T_0T)^{1/2},$$

where T_0 is defined by the relation:

$$\sigma \propto \exp(-T_0/T)^{1/4}.$$

Hence, by comparison with the last section,

$$T_o = (16\alpha^3)/N(E_F)K.$$

IV. DISCUSSION

A. Amorphous Sb

1. Conductivity

To test the hypothesis of variable-range hopping conductivity, the log of the resistance was plotted against $T^{-1/4}$ (Fig. 15 and Fig. 16). The predicted temperature dependence was followed quite well for low temperatures up to about 175 K, where a significant deviation from hopping behavior was noted. Hauser (1973) also found a deviation from $T^{-1/4}$ dependence above about 180 K for evaporated amorphous Sb films, which he attributed to annealing.

The values calculated for T_0 and the density of states, $N(E_F)$, for the various samples are shown in Table 2. These results are in fairly good agreement with Hauser (1).

2. Thermopower

To test the hypothesis of variable range hopping for the thermopower, the Seebeck coefficient was plotted vs. the square root of T. (Figs. 17, 18 and 19). The results here showed considerable deviation between samples. Both the sign and the temperature dependence of the thermopowers of amorphous Ge and Si were found to be strong functions of the preparation conditions by Beyer and Stuke (4). This was attributed to the amount of oxygen present in the films. A Ge film with high oxygen content was found to have a positive Seebeck coefficient over a significant temperature range as compared with a negative Seebeck for more pure Ge. It was suspected that oxygen impurities annihilated local defect states. The change in sign for Sb No. 6, the only one made from a powdered charge which was probably highly oxidized, may be attributable to a similar effect. The calculated slope of the density of states at the Fermi energy for each of the samples is shown in Table 2.

Using the calculated density of states at the Fermi energy, and the calculated slope of the density of states at the Fermi energy, a possible density of states function is sketched in Figure 20. This was done assuming that the density of states function was fairly constant from sample to sample, while the Fermi energy shifted.

B. Amorphous Te

The $T^{-1/4}$ behavior of the conductivity of Te films reported by Phahle (2) was not reproducible here. Te proved to be even more tricky to evaporate than Sb. Out of seven tries, only one successful film was made. Perhaps the film was not amorphous enough to exhibit true hopping conductivity. The thermopower measurements, however, match the general behavior for liquid Se - Te samples reported by Mahdjuri, and the single value reported by Becquerel et al. (4) for Te

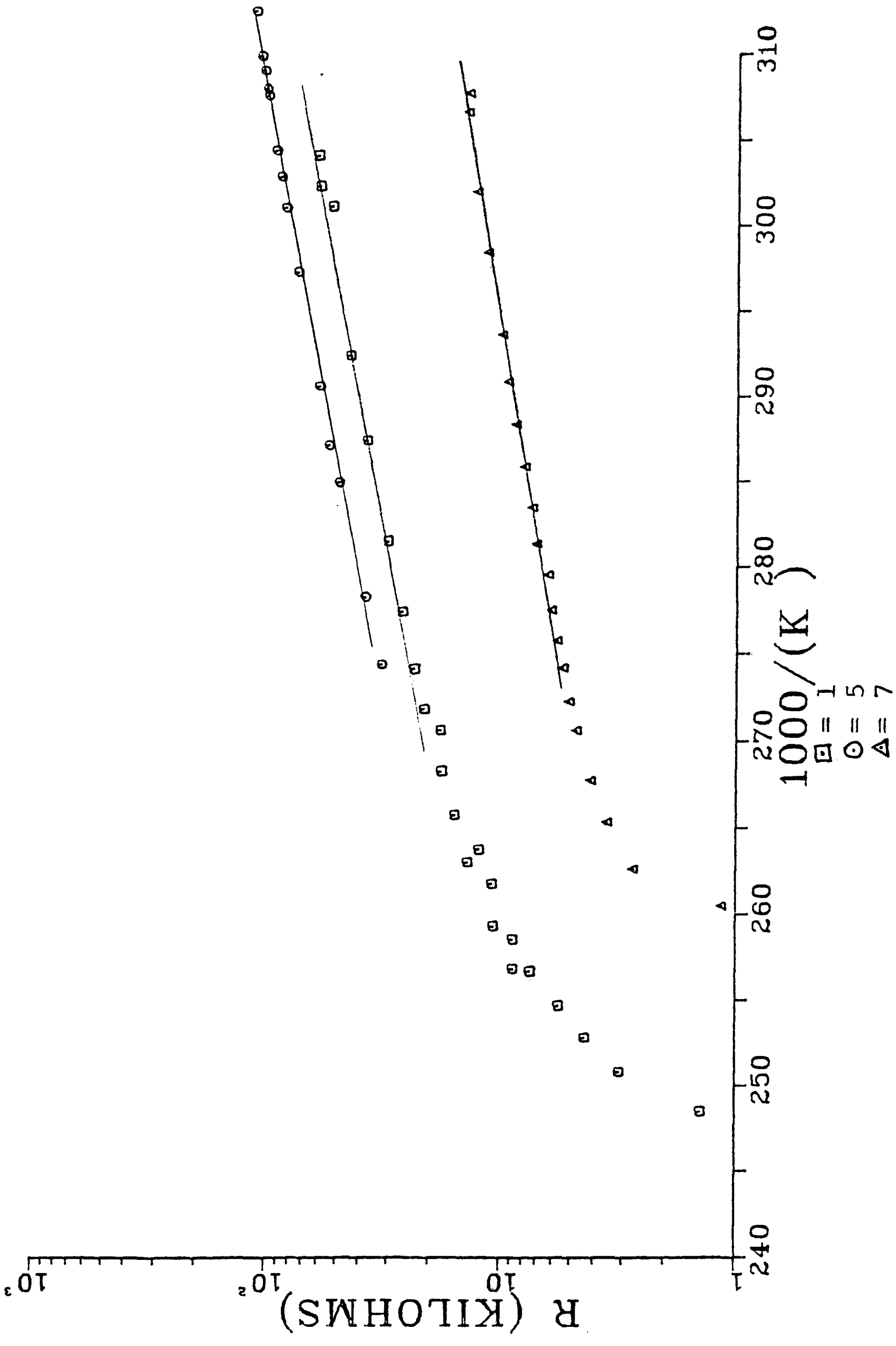

Figure 15: LnR vs. $T^{-1/4}$ Sb No. 1, 5, 7.

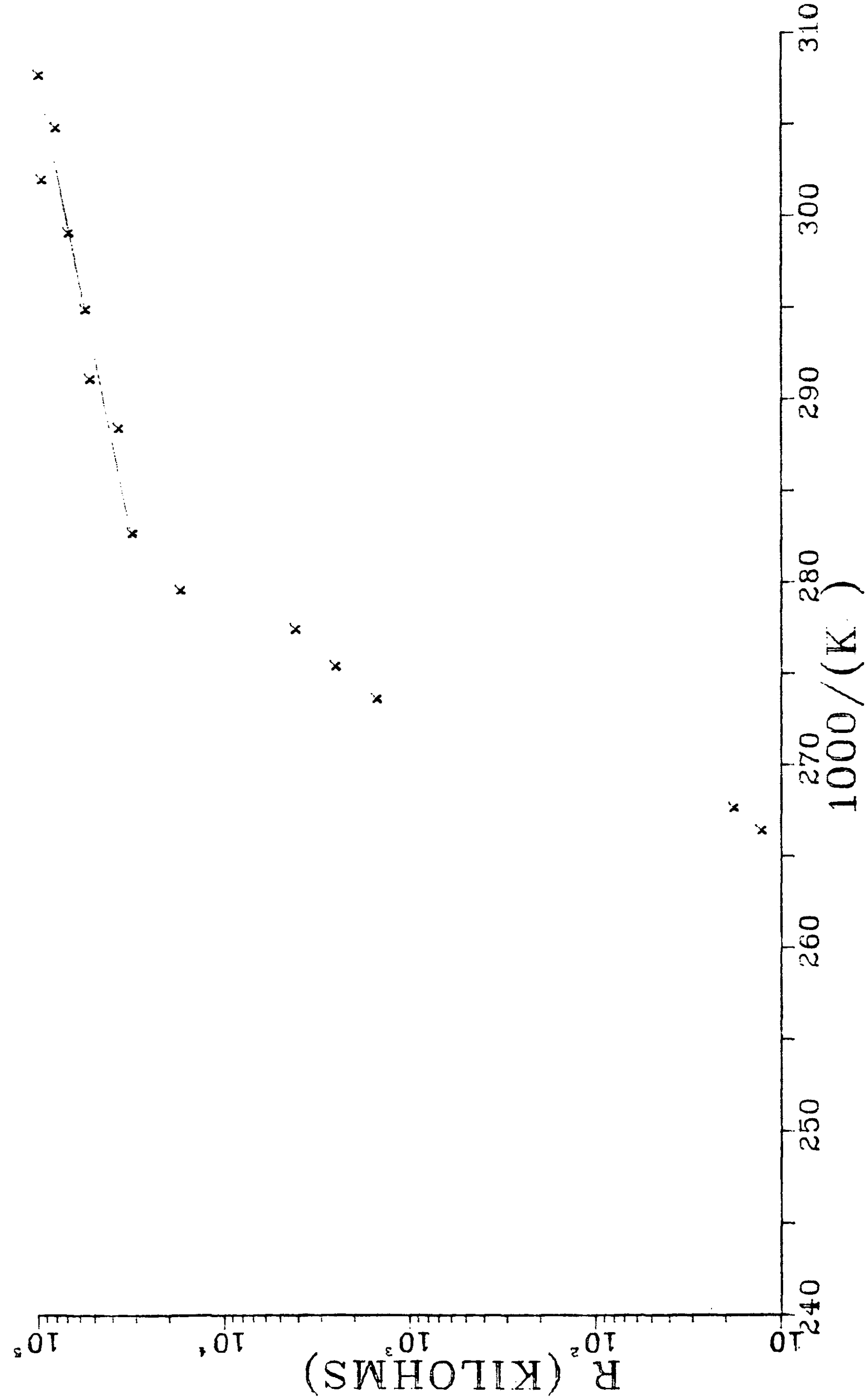

Figure 16: LnR vs. $T^{-1/4}$ for Sb No. 6.

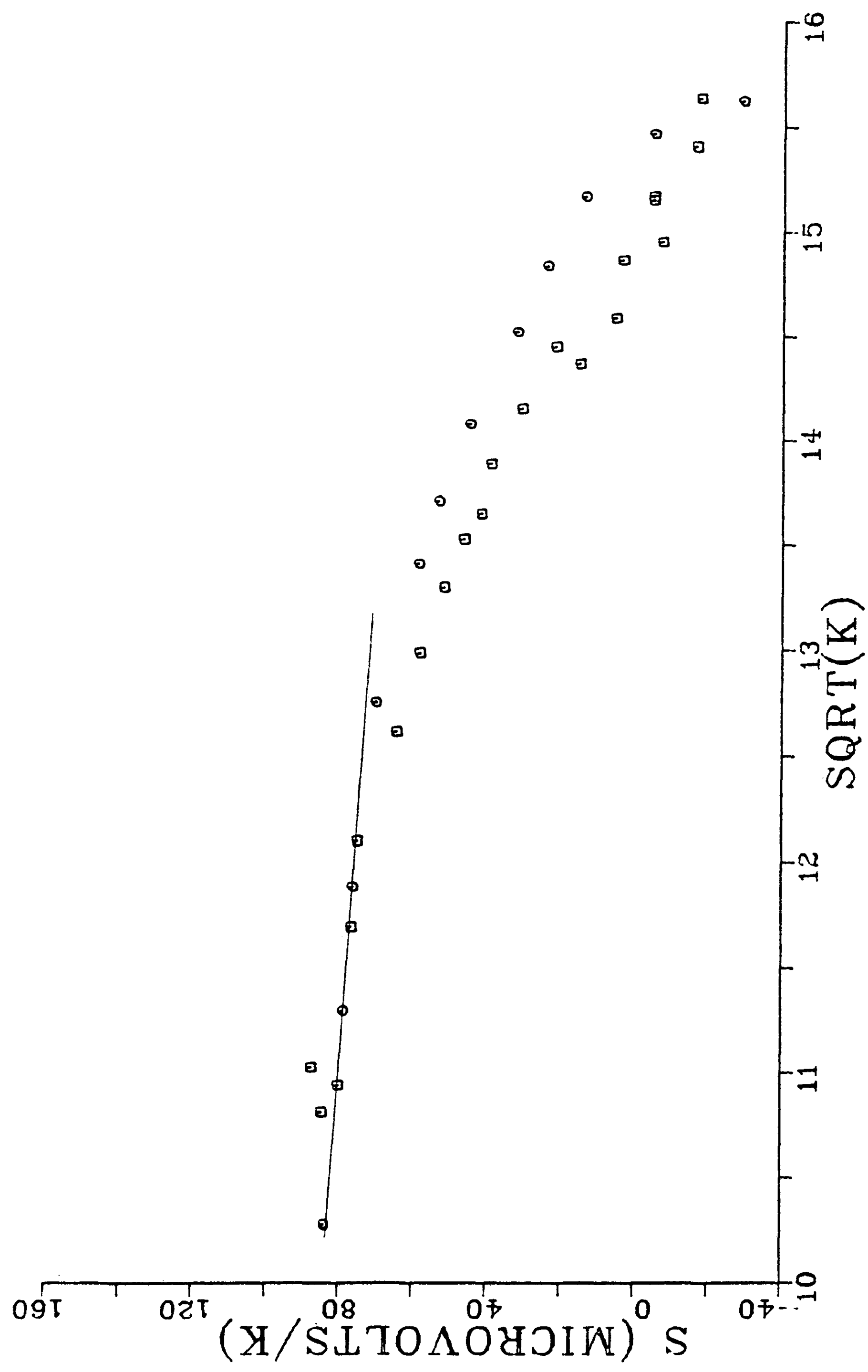

Figure 17: Seebeck vs. $K^{1/2}$ for Sb No. 1,2.

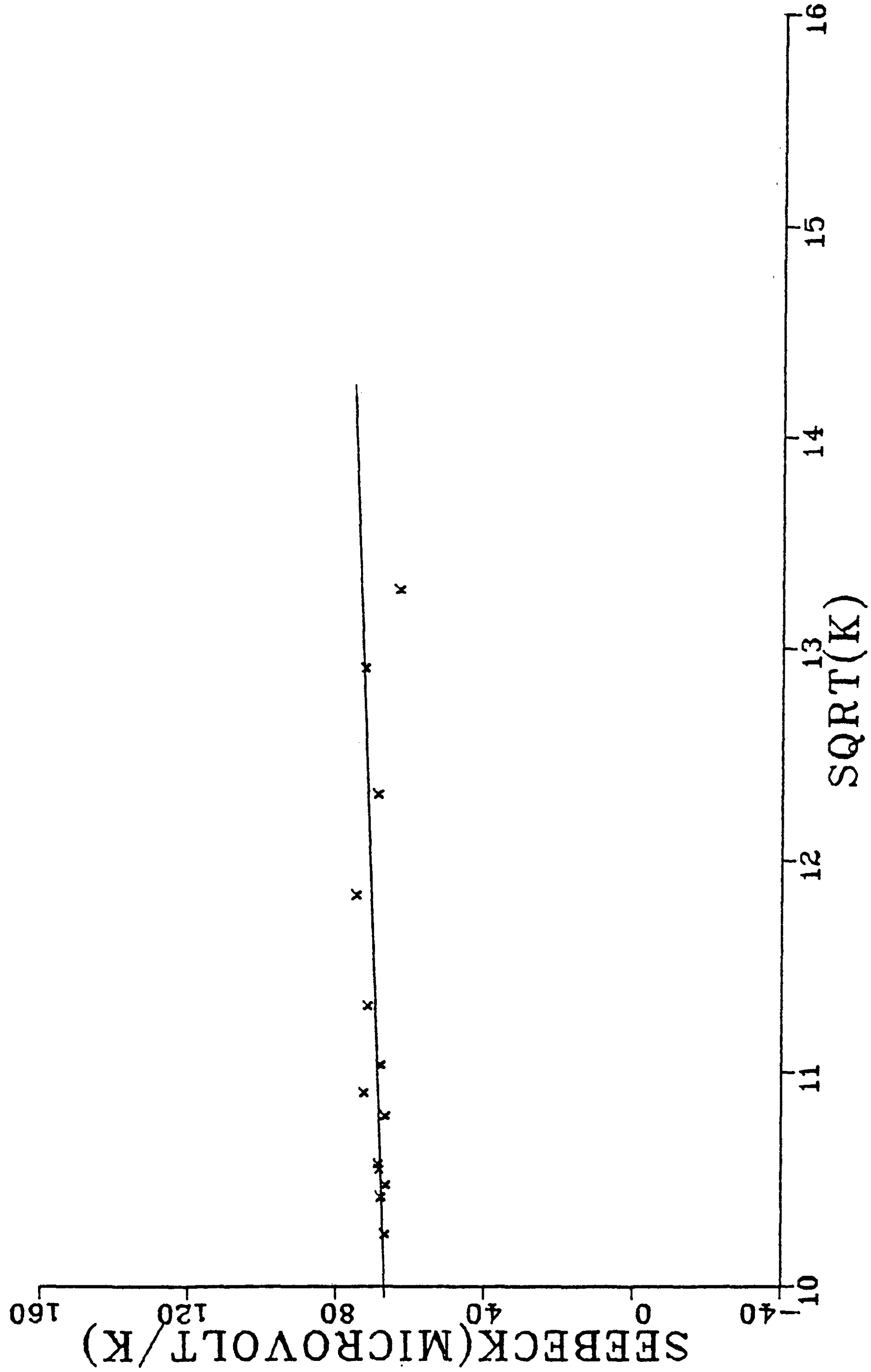

Figure 15: Seebeck Coefficient vs. $T^{1/2}$ for Sb No. 5.

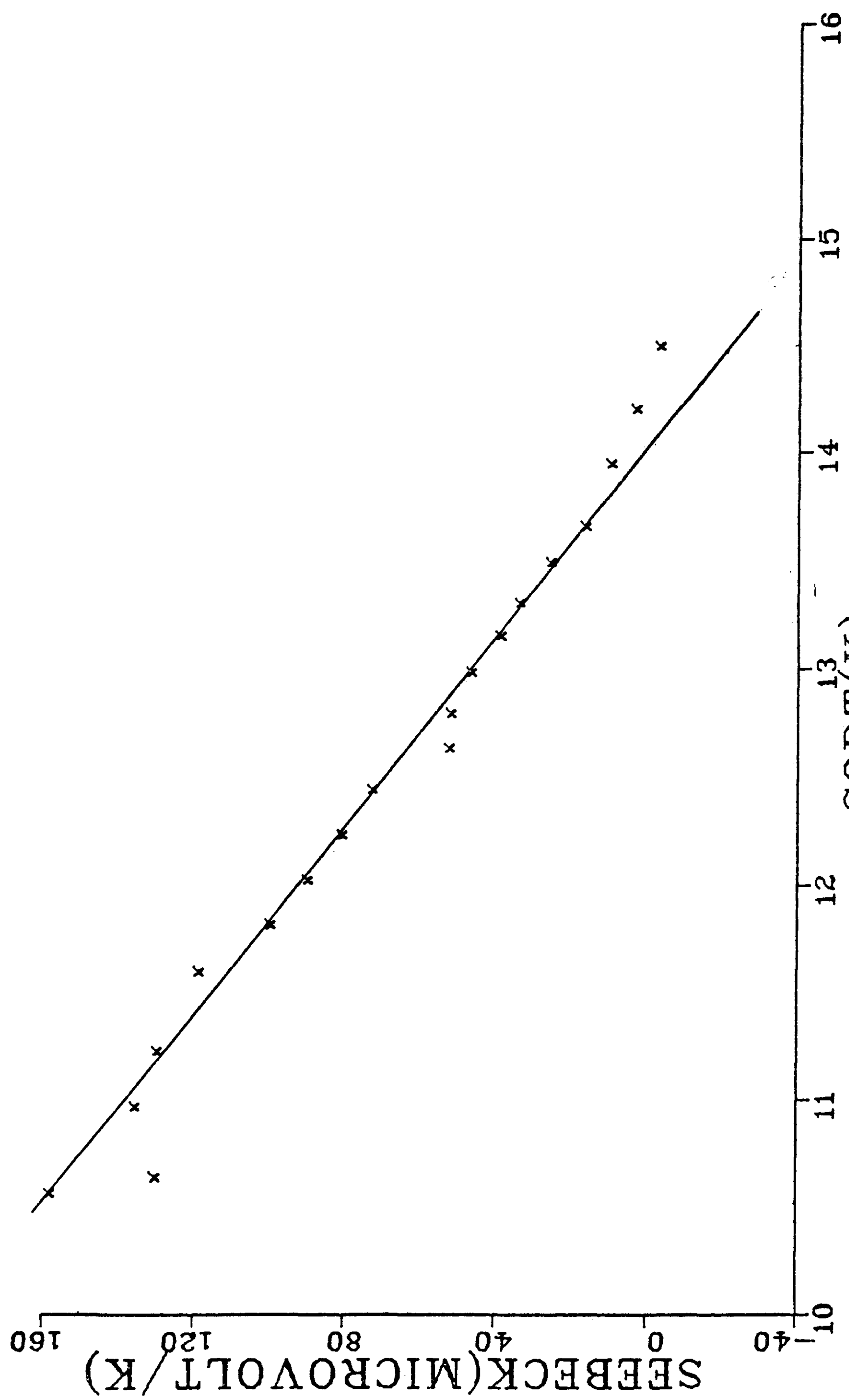

Figure 19: Seebeck Coefficient vs. $T^{1/2}$ for Sb No. 7.

Table 2: Calculated Values of T_o, $N(E_F)$ and $\frac{dN(E_F)}{dE}$.

Sb No.	T_o(K)	$N(E_F)$ (cm^{-3}-eV^{-1})	$\frac{dN(E_F)}{dE}$ (cm^{-3}-eV^{-2})
1	1.30×10^{6}	2.79×10^{20}	-2.96×10^{20}
2	3.10×10^{6}	1.17×10^{20}	-8.04×10^{19}
3	2.52×10^{6}	1.44×10^{20}	-1.38×10^{20}
4	6.74×10^{4}	5.38×10^{21}	- - -
5	8.58×10^{5}	4.23×10^{20}	2.87×10^{20}
6	5.33×10^{6}	6.80×10^{19}	- - -
7	8.23×10^{5}	4.41×10^{20}	-5.88×10^{21}

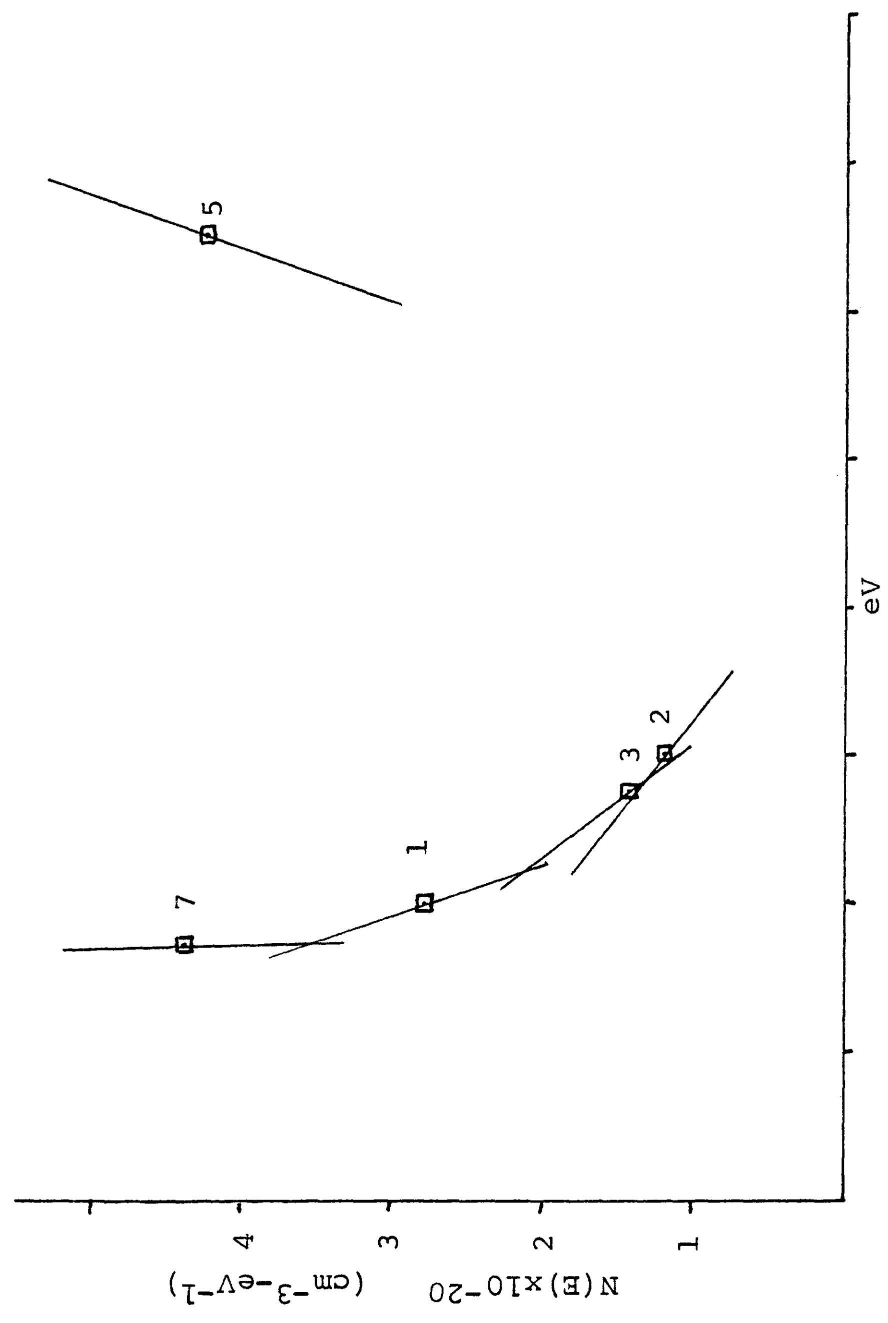

Figure 20: Possible Density of States for Sb.

IV. SUMMARY

The preliminary results quoted in this paper merit further investigation. The resistance results for the amorphous Sb match published data fairly well. The thermoelectric data for amorphous Sb presented here is the first of its kind. Both the thermopower data and the resistance data for amorphous Sb are consistent with the variable-range hopping theory. More work needs to be done to quantify the dependence of the thermopower on evaporation conditions. The apparatus needs to be modified to allow lower temperatures to be reached.

The Te results are even more preliminary, and work still has to be done to find how to reliably produce a good film.

REFERENCES CITED

1. Hauser, J. J., Hopping Condictivity in Amorphous Antimony, Phys. Rev. B, 9, pp. 2623 - 2626, (1974).

2. Phale, A. M., Hopping Conductivity in Amorphous Tellurium Films, Thin Solid Films, 61, pp. L21 - L22, (1979).

3. Mott, N. F. and Davis, E. A., Electronic Processes in Non-Crystalline Materials, Oxford, Clarendon Press, pp. 7 - 64, (1979).

4. Beyer, W. and Stuke, J., Thermoelectric Power of Amorphous Ge and Si, 5th Int. Conf. on Amorphous and Liquid Semiconductors, pp. 251-258, (1973).

5. Becquerel, Mattheissen and Tait, Smithsonian Physical Tables, 9th ed., p. 380, (1959).

Appendix A

Sample Calculations

Below are shown the raw data and the method of calculation for a single set of readings. This method was used for all of the data in this paper.

Reference junction temperature = 28.2°C

	a	b	c	d
I (μV)	-7892	7895	-7846	7847
II (μV)	-7196	7194	-7167	7172
III (μV)	760	-766	747	-749
IV (μV)	1458	-1458	1434	-1438
V (KΩ)	30.360	30.277		
VI (KΩ)	30.340	30.281		
VII (Ω)	29.284	34.550		
VIII (Ω)	39.859	39.205		

Readings were taken in the order Ia, Ib, IIa, IIb, etc. for columns a and b. Readings in columns c and d were taken in the order IVd, IVc, IIId, IIIc, etc. Row I represents the thermoelectric voltage of the 'left' thermocouple relative to the reference junction and row II represents that of the 'right' thermocouple. Row III represents the thermoelectric voltage induced in the sample relative to Chromel, and row IV the same relative to Constantan. Rows V and VI are the resistance readings across the sample through the Chromel and Constantan leads, respectively. Rows VII and VIII are the resistances through each of the two thermocouples with their leads.

To obtain the temperature of the 'left' side of the sample, the temperature of the reference junction was converted to a voltage using standard tables (Omega) and linear interpolation. In this way, for example, 28.2^{o}C converts to 1690μV relative to 0^{o}C. The readings of row I were then averaged and adjusted relative to 0^{o}C using the Omega tables. For the sample readings, therefore, we obtain the following:

$$\frac{-7892-7895-7846-7847}{4} + 1690 = -6180\,\mu V$$

$$-6180\,\mu V \text{ converts to } -121.76^{o}C = T_\ell$$

The same operation was performed on Row II to obtain the temperature of the 'right' side:

$$\frac{-7196-7194-7167-7172}{4} + 1690 = -5492\,\mu V$$

$$-5492\,\mu V \text{ converts to } -105.71^{o}C = T_r$$

The next step was to compute the temperature difference across the sample:

$$T_r - T_\ell = 16.05^{o}C = \Delta T$$

and the average temperature:

$$(T_r + T_\ell)/2 = -113.74^{o}C = T_{av}$$

The thermopower relative to Chromel was then calculated by dividing T into the average of row III:

$$\Delta V/\Delta T \text{ (Chromel)} = (760 + 766 + 747 + 749)/4(16.05) = 47.07\,\mu V/K$$

The thermopower relative to Constantan was similarly calculated from row IV:

$$\Delta V/\Delta T\text{(Constantan)} = (1458 + 1458 + 1434 + 1438)/4(16.05) = 90.16\,\mu V/K$$

Using the known thermopowers of Chromel and of Constantan, these two thermopowers were then converted to absolute and averaged together:

$$47.07 + 17.88 = 64.07\,\mu V/K \text{ (Chromel)}$$

$$\text{and: } 90.16 - 25.50 = 64.66\,\mu V/K \text{ (Constantan)}$$

$$\text{giving: } (64.07 + 64.66)/2 = 64.37\,\mu V/K$$

Note that these two calculated thermopowers are within one percent of each other; this is a typical case.

The resistance of the sample was calculated, assuming negligible resistance between the thermocouple junction and the copper plates, by subtracting the resistance of the leads from the total resistance and averaging:

$$(30{,}360 + 30{,}270 + 30{,}240 + 30{,}281 - 30 - 35 - 34 - 39)/4 = 30.25\ K\Omega$$

Hence, the reported results:

$$T_{av} = -113.74^{o}C = 159.26K$$

$$S = 64.37\,\mu V/K$$

$$R = 30.02\ K\Omega$$

Appendix B

Tabulation of Data

Table 3: Resistance and Seebeck vs. T for Sb No. 1

T(K)	S(μV/K)	R
116.93	84.38	61.05KΩ
121.63	87.17	53.01
119.72	79.86	59.95
136.78	76.51	44.14
146.51	74.97	37.38
159.24	64.37	30.32
168.80	58.04	26.25
176.97	51.54	23.25
183.05	46.16	21.14
192.97	38.86	17.79
200.47	30.61	15.66
208.91	21.39	13.74
221.09	3.23	10.62
229.77	-4.83	8.78
186.31	41.55	17.99
206.59	14.97	12.29
212.92	5.18	10.79
223.74	-7.36	8.795
230.24	-4.89	7.412
237.56	-16.56	5.617
244.70	-17.53	4.334
252.59	-16.13	3.084
262.29	-7.16	1.395
274.55	17.98	46.67Ω
284.35	18.17	46.24
294.12	19.00	46.51
315.11	19.44	47.92
165.03	10.80	43.75
185.02	11.03	20.44
206.19	12.23	29.04
238.52	17.14	30.02
256.18	19.06	29.86
267.30	19.95	30.15
320.57	24.68	31.43

Table 4: Resistance and Seebeck vs. T for Sb No. 2

T(K)	S(μV/K)	R(KΩ)
105.65	83.70	100.40
127.62	78.64	65.48
141.23	76.04	50.20
162.78	69.92	33.57
179.94	58.47	24.89
188.00	53.08	17.40
198.31	44.61	14.75
211.00	31.86	12.06
220.33	23.73	10.34
230.24	13.64	8.838
239.45	-4.97	4.792
244.32	-29.06	2.373
248.74	-28.79	1.656
255.57	-10.07	0.760
263.60	16.98	0.183
269.62	17.47	0.183
314.76	18.78	0.250
282.91	18.05	0.253
117.35	7.39	0.207
168.93	11.00	0.211
219.91	14.70	

Table 5: Resistance and Seebeck vs. T for Sb No. 3.

T(K)	S(μV/K)	R(KΩ)
131.38	100.09	81.85
135.65	92.20	77.28
111.58	110.43	131.19
141.72	101.73	64.97
131.46	105.11	81.94
159.22	87.61	45.62

Table 6: Resistance and Seebeck vs. T for Sb No. 4.

T(K)	S(μV/K)	R(KΩ)
107.64	-280.05	15.64
114.33	-333.17	14.42
180.57	-176.83	11.29
118.72	-173.46	13.32
135.67	-153.58	11.79
150.76	-245.49	10.91
159.51	-168.90	9.563
175.52	-192.48	8.670
186.34	-123.73	7.991

Table 7: Resistance and Seebeck vs. T for Sb No. 5.

T(K)	S(μV/K)	R(KΩ)
108.48	67.86	107.56
104.97	66.73	113.57
118.88	72.46	87.67
109.67	66.40	104.00
111.76	68.59	100.24
116.54	66.65	92.53
121.78	67.95	83.61
128.05	71.48	74.04
140.16	74.76	59.61
151.69	68.93	49.12
166.68	72.56	37.81
176.35	63.24	32.13
113.21	68.30	101.77
147.10	66.66	54.33

Table 8: Resistance and Seebeck vs. T for Sb No. 6

T(K)	S(μV/K)	R
111.58	Resistance	100MΩ
115.82	too	80.6
120.22	high	96.2
124.96		69.0
132.18		55.9
139.21		52.9
144.48		37.0
156.61		31.3
163.66		17.2
168.69		4.10
173.72		2.5
178.29		1.50
193.05		43.89KΩ
194.75		17.93
198.40		12.66

Table 9: Resistance and Seebeck vs. T for Sb No. 7

T(K)	S(μV/K)	R
111.53	157.93	13.96KΩ
113.14	129.99	14.00
120.24	135.44	12.85
126.06	129.60	11.53
134.55	118.49	9.95
139.70	99.51	9.39
144.64	89.66	8.67
149.70	80.47	7.97
154.87	72.39	7.40
159.63	52.24	7.08
163.71	51.84	6.31
168.58	46.35	6.12
172.93	38.61	5.76
176.90	33.54	5.43
181.94	25.42	5.12
186.43	16.27	4.76
194.59	9.62	4.12
201.76	2.97	3.51
210.20	-3.31	2.71
217.17	3.19	1.14
224.54	14.37	63.39Ω
234.72	18.24	29.00
243.80	21.02	19.40
249.36	21.02	15.51

Table 10: Resistance and Seebeck vs. T for Te No. 1

T(K)	S(μV/K)	R(KΩ)
134.68	188.57	1,477
133.71	217.38	1,523
125.00	77.76	1,645
144.24	178.60	1,530
186.71	336.23	1,259
219.40	399.63	1,022
241.12	438.79	854
260.20	471.27	678
282.37	481.03	511
305.03	471.55	434
336.42	400.24	88.5

Appendix C

The thermocouples were checked for accuracy at low temperature by immersion in LN_2 at the boiling point. The calculated temperatures for each thermocouple are shown in Table 11 for three trials. The error in the thermocouple readings was thus estimated to be less than 1K. The Seebeck coefficient of polycrystalline Sb No.s 1 and 2 is compared with that of bulk antimony in Fig. 21. The Seebeck coefficient measured on the evaporation rig is compared with that measured in the cryostat of the same laboratory of a standard Bi sample in Fig. 22.

Table 11: Calibration of Thermocouples by Immersion in LN_2

Trial No.	T_1(k)	T_2(k)
1	74.92	75.19
2	75.08	75.19
3	75.19	75.27

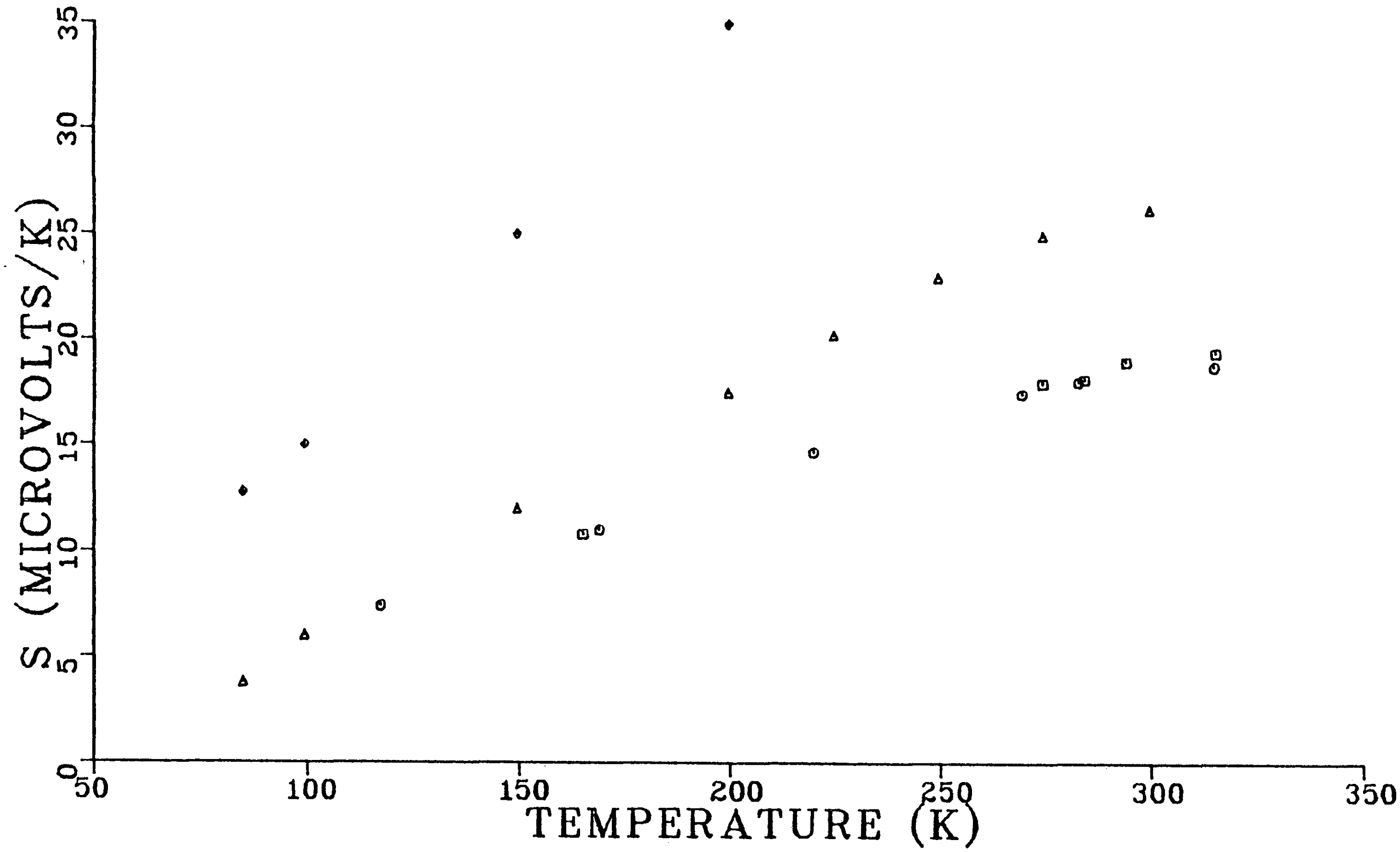

Figure 21: Comparison of Polycrystalline Sb with Bulk Seebeck. (□ = No. 1, ⊙ = No. 2, △ = ∥, ◇ = ⊥).

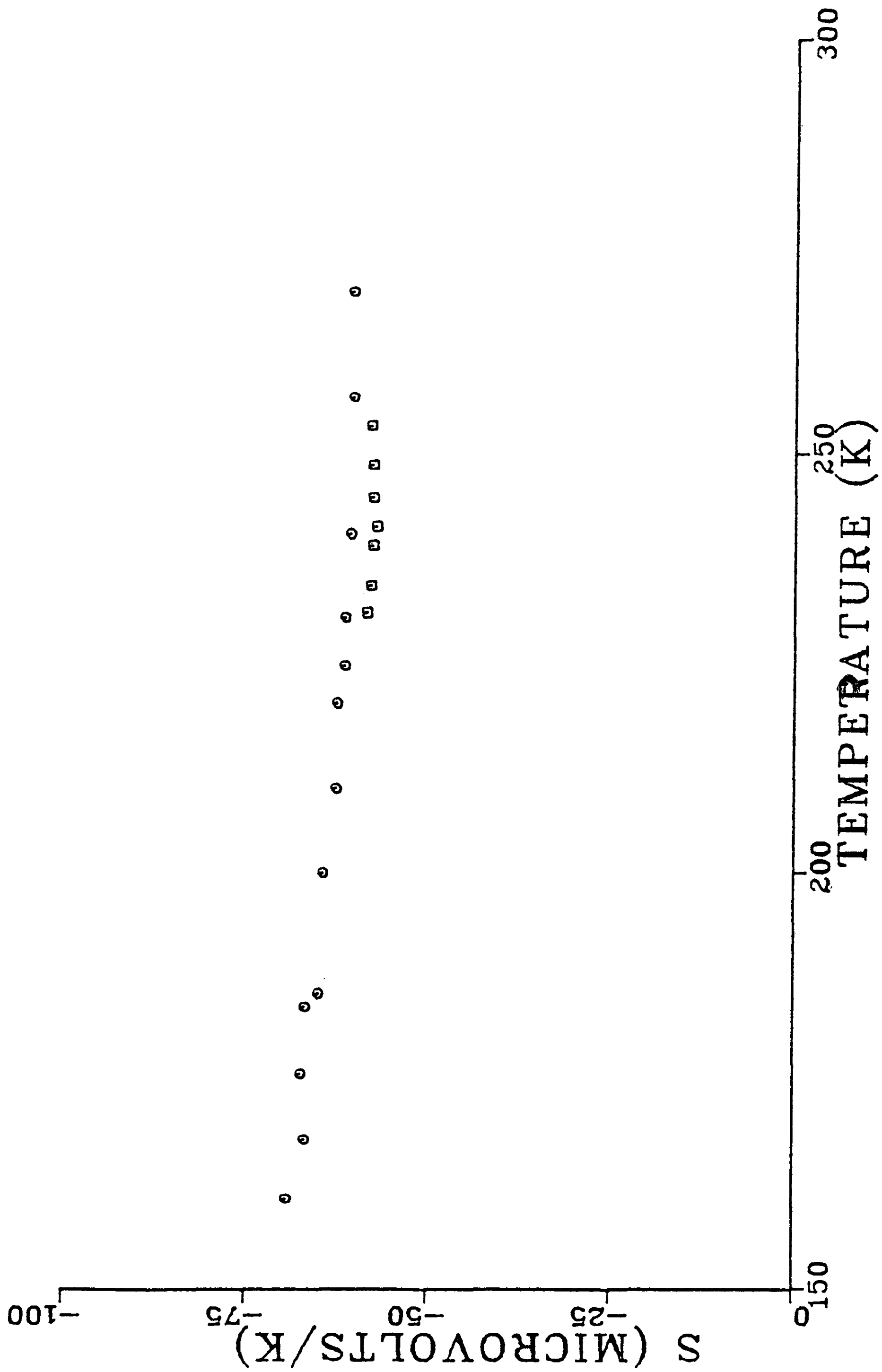

Figure 22: Comparison of Seebeck Obtained from Two Different Apparatus. (⊙ from evaporator device, ⊡ from cryostat.)

Appendix D

Boat Power vs. Variac Setting

Variac Setting	Voltage rms (volts)	Current rms (amps)	Power rms (watts)
25	1.0	7.0	7.0
30	1.2	8.5	10.2
35	1.4	11.0	15.4
40	1.5	12.5	18.8
45	1.7	13.0	22.1
50	1.9	13.5	25.7